

---

# Composing Linear Layers from Irreducibles

---

Travis Pence, Daisuke Yamada, Vikas Singh

University of Wisconsin–Madison  
Madison, WI

{tnpence, dyamada2}@wisc.edu, vsingh@biostat.wisc.edu

## Abstract

Contemporary large models often exhibit behaviors suggesting the presence of low-level primitives that compose into modules with richer functionality, but these fundamental building blocks remain poorly understood. We investigate this compositional structure in linear layers by asking: *can we identify/synthesize linear transformations from a minimal set of geometric primitives?* Using Clifford algebra, we show that linear layers can be expressed as compositions of bivectors—geometric objects encoding oriented planes—and introduce a differentiable algorithm that decomposes them into products of rotors. This construction uses only  $\mathcal{O}(\log^2 d)$  parameters, versus  $\mathcal{O}(d^2)$  required by dense matrices. Applied to the key, query, and value projections in LLM attention layers, our rotor-based layers match the performance of strong baselines such as block-Hadamard and low-rank approximations. Our findings provide an algebraic perspective on how these geometric primitives can compose into higher-level functions within deep models.

## 1 Introduction

There is growing consensus [Kozachkov et al., 2023] that, like biological systems, modern models may internally rely on *low-level primitives* that *compose* to form modules with more complex functionality [Weiss et al., 2021]. This compositional perspective was one motivation behind capsule networks [Sabour et al., 2017], which explicitly modeled part-whole relationships through vector-based capsules. But the task of localizing and characterizing such primitives remains challenging albeit interesting. A general capability to compose pre-trained modules in a prescribed way could, in principle, lead to a larger model with predictable and more controllable functionality [Zou et al., 2025, Schug et al., 2024, Ghazi et al., 2019, Abnar et al., 2023, Press et al., 2023], with potential applications ranging from safety guardrails to interpretability.

Some recent results suggest some progress in this direction. In mixture-of-experts architectures [Masoudnia and Ebrahimpour, 2014, Riquelme et al., 2021], specialized sub-networks are conditionally activated and composed via routing [Büchel et al., 2025]. Model merging has evolved from simple parameter averaging to more sophisticated alignment of different model latent representations [Lähner and Moeller, 2024]. Fine-tuning methods like LoRA [Hu et al., 2021] implicitly assume that low-dimensional adjustment of a base network should suffice—essentially a two-level composition. Each approach offers a distinct perspective on composition but are not focused on addressing how the mechanistic composition of low-level primitives gives more complex behavior. To this end, mechanistic interpretability [Rai et al., 2024] and neurosymbolic methods [Yang and Chaudhuri, 2022] explore this space, but are still in a nascent stage of development.

**Scope of this paper.** Consider a core module—with millions of parameters—in a large model. *Can we synthesize its functionality from its most basic primitives? How many such objects would we need?* This casts our broader interest in composition into a concrete problem: *identifying a minimal set of irreducibles that combine in specific ways to realize the full functionality of the module*. We study this problem for *linear layers*—noting that linear layers make up a large portion of parameters in large

language models (LLMs). While prior work suggests various parameter-efficient approximations, our interest is not only function approximation, rather to build up the functionality by characterizing its *algebraic structure*. To formalize the above intuition, we use the language of *Clifford algebra*, where linear transformations naturally decompose into simple *bivectors*—geometric objects representing oriented planes. This view reveals how the functionality of a linear layer can be synthesized as a structured composition of a few hundred geometric objects (parameters).

Our key **contributions** are: **(a)** We express linear transformations as compositions of geometric primitives—specifically, bivectors in Clifford algebra—using rotor sandwich products acting on local subspaces of an input multivector. This requires  $\mathcal{O}(\log^2 d)$  scalar parameters, compared to  $\mathcal{O}(d^2)$  for dense layers, where  $d$  is the input/output dimension. **(b)** We propose a differentiable invariant decomposition algorithm that maps bivectors to their corresponding rotors in closed-form, which enables integration with autograd and gradient-based optimization. **(c)** Empirically, we replace the key, query, and value projections in LLM attention layers and show comparable downstream performance in accuracy and perplexity across various datasets.

Our goal is to show the *feasibility* of this algebraic decomposition approach. It is not a drop-in replacement, since practical benefits will require additional system-level integration beyond the scope of this work. The focus here is on the underlying algorithmic and mathematical foundations.

## 2 Preliminaries

We review some relevant concepts from Clifford algebra (also see Hestenes and Sobczyk [2012]).

**Clifford algebra.** A *Clifford algebra*,  $\text{Cl}_{p,q}(\mathbb{R})$ , is an associative algebra over  $\mathbb{R}^n$  equipped with a quadratic form of signature  $(p, q)$ , where  $n = p + q$ . The algebra admits two basic products: the *inner product* and *outer (wedge) product*, denoted by  $\cdot$  and  $\wedge$  respectively. Their sum defines the *geometric product*, which for vectors  $u, v \in \mathbb{R}^n$  takes the form:

$$uv \triangleq u \cdot v + u \wedge v.$$

The algebra is generated by orthogonal basis vectors  $e_1, \dots, e_n$ , called *generators*, satisfying:

$$e_i^2 = +1 \quad \text{for } 1 \leq i \leq p; \quad e_j^2 = -1 \quad \text{for } p < j \leq n; \quad e_i \wedge e_j = -e_j \wedge e_i \quad \text{for } i \neq j.$$

These relations encode the metric and orientation of the underlying space. The algebra has a canonical basis of  $2^n$  elements: the scalar 1 and all distinct products of the basis vectors  $e_1, \dots, e_n$ . In particular, *basis bivectors* are wedge products of two distinct basis vectors, i.e.,  $e_i \wedge e_j = e_i e_j$  for  $i < j$ . More generally, *basis k-vectors* are wedge products of  $k$  distinct basis vectors (see Fig. 1), and there are  $\binom{n}{k}$  such elements for each  $k$ . The total number of such basis elements is the *dimension* of the algebra. The *reversion*, given by  $\dagger$ , reverses the order of basis vectors. For example,  $(e_1 e_2)^\dagger = e_2 e_1$  and  $(e_1 e_2 e_3)^\dagger = e_3 e_2 e_1$ .

The algebra decomposes into a direct sum of subspaces indexed by *grade*: scalars (grade 0), vectors (grade 1), *bivectors* (grade 2), and general *k-vectors*, which are linear combinations of corresponding basis elements. A *multivector* is a general element of  $\text{Cl}_{p,q}(\mathbb{R})$ , expressed as a linear combination of components of multiple grades. For example,  $e_1 e_2$  is a basis bivector;  $e_1 e_3 + 2e_2 e_3$  is a bivector; and  $1 + (2e_2 + e_4) - e_1 e_3$  is a multivector composed of elements of grades 0, 1, and 2. We denote the subspaces of vectors and bivectors by  $\text{Cl}^1(\mathbb{R})$  and  $\text{Cl}^2(\mathbb{R})$ , and more generally,  $\text{Cl}^k(\mathbb{R})$  for grade- $k$  elements. The algebra naturally splits into *even* and *odd* subalgebras based on grade parity. The *even subalgebra*  $\text{Cl}^+(n) \subset \text{Cl}(n)$  consists of elements of even grade (scalars, bivectors, 4-vectors, etc), while odd elements include vectors, trivectors, and so on. Some well-known algebraic systems arise as special cases of Clifford algebras: the real numbers  $\mathbb{R} \cong \text{Cl}_{0,0}(\mathbb{R})$ , the complex numbers  $\mathbb{C} \cong \text{Cl}_{0,1}(\mathbb{R})$ , the quaternions  $\mathbb{H} \cong \text{Cl}_{0,2}(\mathbb{R})$ , and the hyperbolic numbers  $\text{Cl}_{1,0}(\mathbb{R})$ . This way, Clifford algebras naturally generalize familiar algebraic systems by incorporating geometric structure. To keep notations short, we write  $\text{Cl}_{p,q}(\mathbb{R})$  as  $\text{Cl}(p, q)$  and only consider  $\text{Cl}(n, 0)$ , denoted as  $\text{Cl}(n)$ .

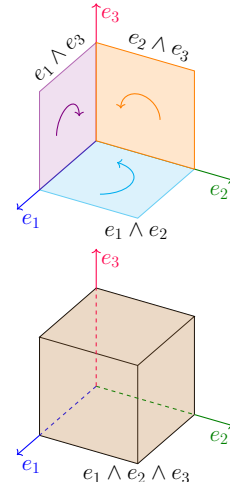


**Figure 1:** The basis vectors, bivectors, and trivector for  $\text{Cl}(3)$ . The top part shows a 3D coordinate system with basis vectors  $e_1$  (blue),  $e_2$  (green), and  $e_3$  (red). It highlights three bivectors:  $e_1 \wedge e_2$  (purple plane),  $e_2 \wedge e_3$  (orange plane), and  $e_1 \wedge e_3$  (cyan plane). The bottom part shows a 3D cube representing the trivector  $e_1 \wedge e_2 \wedge e_3$  (brown).

### 3 Algebraic Structure of Rotor-based Transformations

We aim to describe standard linear transformations in terms of the algebraic structure of Clifford algebra. We begin by noting how any linear map can be expressed as a sum of multivector products, and then show how restricting to rotors in the Spin group is helpful.

**Clifford form of linear transformations.** A linear map between two vector spaces is one that preserves additivity and homogeneity. Traditionally, such transformations are represented as dense matrices with independent parameters. In contrast, we consider  $\text{Cl}(n)$  and write these transformations in terms of the geometric product between multivectors—algebraic objects that encode both magnitude and orientation. We first restate a textbook result.

**Lemma 1.** (Hestenes and Sobczyk [2012]) *Let  $a_w$  and  $b_w$  denote multivectors in  $\text{Cl}(n)$ . Any linear function  $F$  from  $\text{Cl}^k(n)$  to  $\text{Cl}(n)$  can be written as the finite sum*

$$F(x) = \sum_w a_w x b_w. \quad (1)$$

This result shows that linear transformations in Clifford algebra can be expressed as products involving multivectors acting from both the left and right. Thus, Clifford algebra gives us a way to represent a general, arbitrary linear map. But there is a cost: arbitrary multivectors have too much freedom and require all  $2^n$  parameters of the full Clifford algebra, which makes the representation inefficient. We will constrain  $a_w$  and  $b_w$  to preserve *rotational symmetries*, leading to the Spin group

$$\text{Spin}(n) \triangleq \{r \in \text{Cl}^+(n) \mid rr^\dagger = 1\}$$

where  $\text{Cl}^+(n) \subset \text{Cl}(n)$  is the even subalgebra and  $\dagger$  denotes grade-wise reversion. The Spin group captures the set of orientation-preserving rotations within  $\text{Cl}(n)$ . The elements  $r \in \text{Spin}(n)$ , called *rotors*, act on multivectors  $x \in \text{Cl}(n)$  through the sandwich product as shown in Fig. 2,

$$x \mapsto r x r^\dagger. \quad (2)$$

Applying multiple rotors in *parallel* instantiates Lem. 1, where  $a_w = r_w$  and  $b_w = r_w^\dagger$ . While this sandwich form is useful, we must efficiently parametrize these rotors. To do so, we first observe the relationship between  $\text{Spin}(n)$  and the more familiar rotation group,  $\text{SO}(n)$ .

**Fact 1.**  $\text{Spin}(n)$  is a double cover of the special orthogonal group  $\text{SO}(n)$ .

This relationship is important in that while  $\text{Spin}(n)$  and  $\text{SO}(n)$  are topologically different (hence the “double cover”), they share the same infinitesimal structure—namely, their Lie algebra. This allows using parametrization techniques for  $\text{SO}(n)$  to represent elements of  $\text{Spin}(n)$ . In particular, we will see that rotors can be generated from bivectors via the exponential map, just as rotation matrices arise from skew-symmetric matrices.

**Remark.** For vector inputs  $x$ , the sandwich product  $r x r^\dagger$  performs the same rotation as the corresponding matrix in  $\text{SO}(n)$ . However, the full utility of rotors becomes clear when  $x$  is multivector: the transformation extends to higher-grade components within the Clifford algebra, going beyond the vector subspace. This makes rotors especially suitable for operating on the richer representations.

We return to the question: can we efficiently represent rotors so that  $a_w, b_w$  in Lem. 1 belong to  $\text{Spin}(n)$ ?

**Constructing rotors from bivectors.** Rotors in  $\text{Spin}(n)$  can be parametrized via bivectors: grade-2 elements of  $\text{Cl}(n)$  that encode oriented planes of rotation. To understand this parametrization, we examine the connection between rotors and rotation matrices via Lie groups and their Lie algebras.

**Definition 1.** A Lie group  $G$  is a smooth manifold with the usual group properties along with smooth (infinitely differentiable) group operations. Its associated Lie algebra is a vector space equipped with an antisymmetric, bilinear operation  $[X, Y]$ , called the Lie bracket, satisfying the Jacobi identity.

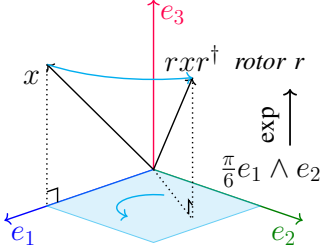


**Figure 2:** The sandwich product rotating a vector  $60^\circ$  in the  $e_1 \wedge e_2$  plane.

Let us check examples.  $\text{Spin}(n)$  and  $\text{SO}(n)$  are different Lie groups with the same Lie algebra. Specifically, the Lie algebra of skew-symmetric matrices,  $\mathfrak{so}(n) \triangleq \{B \in \mathbb{R}^{n \times n} | B = -B^T\}$ , underlies both  $\text{Spin}(n)$  and  $\text{SO}(n)$ , despite their topological differences. This shared structure is important. The exponential map gives a surjective correspondence between  $\mathfrak{so}(n)$  to  $\text{SO}(n)$  as

$$\exp(B) = \sum_{i=0}^{\infty} \frac{B^i}{i!}, \quad (3)$$

showing that every rotation in  $\text{SO}(n)$  can be realized as  $\exp(B)$  for some  $B \in \mathfrak{so}(n)$  using only  $\dim(\mathfrak{so}(n)) = \binom{n}{2}$  independent parameters—fewer than the  $n^2$  entries of a matrix [Lezcano-Casado and Martínez-Rubio, 2019]. The bridge to the Clifford algebra setting is from another key isomorphism:

**Fact 2.** *The space of skew-symmetric matrices is isomorphic to that of bivectors, i.e.,  $\mathfrak{so}(n) \cong \text{Cl}^2(n)$ .*

Given a skew-symmetric matrix  $B \in \mathfrak{so}(n)$ , the corresponding bivector  $b \in \text{Cl}^2(n)$  is constructed as

$$b = \sum_{1 \leq i < j \leq n} B_{i,j} e_i \wedge e_j.$$

Similar to the exponential map relating  $\mathfrak{so}(n)$  and  $\text{SO}(n)$  (i.e.,  $\exp(B)$  generating rotations in  $\text{SO}(n)$ ), every rotor  $r \in \text{Spin}(n)$  is the exponential of some bivector  $b \in \text{Cl}^2(n)$  given explicitly by the series

$$r = \exp(b) = \sum_{i=0}^{\infty} \frac{b^i}{i!}, \quad (4)$$

where  $b^k$  is the  $k$ -fold geometric product of  $b$  with itself. This means that we can encode a rotor with only  $\dim(\text{Cl}^2(n)) = \binom{n}{2}$  parameters—the dimension of the bivector space.

**Main advantage.** At first glance, our parametrization may seem to offer no advantage. We have parametrized both  $\text{Spin}(n)$  and  $\text{SO}(n)$  from the same  $\binom{n}{2}$  parameters from  $\mathfrak{so}(n)$ . Notice that while  $\text{SO}(n)$  acts only on  $n$ -dimensional vectors, our rotors in  $\text{Spin}(n)$  act on a subset of the full  $2^n$ -dimensional space of multivectors. By utilizing *rotors as the action on multivector input and bivectors as our irreducible primitives*, we will use exponentially fewer parameters.

**Example 3.1.** *A  $d \times d$  dense matrix with  $d = 2048$ , common in self-attention blocks and projection layers (e.g., in LLaMA), uses more than 4M parameters. If  $w$  (e.g.,  $\simeq 3$ ) is the width hyperparameter in Lem. 1, approximating with bivector irreducibles requires only  $w \left( \frac{\log_2 d}{2} \right) = 55 w$ .*

This reduction (to  $55 \times 3$ ) comes from identifying bivectors as the primitive that generate rich linear maps through composition. Note that the infinite series in (4) is problematic due to the need for approximation. We avoid this by presenting a closed-form solution that preserves differentiability.

## 4 Algorithmic Implementation and Analysis of our Rotor-gadget

We discussed how rotors can be parametrized through bivectors via the exponential map in (4). A remaining challenge is the infinite series. Of course, we can truncate to a finite length and incur approximation errors. However, for a special class of bivectors, the exponential map admits an exact closed-form solution, which prevents any approximation errors. Moreover, this form remains fully differentiable. We describe the details of this alternative here.

### 4.1 Closed-form differentiable computations of rotors

A key observation is that when a skew-symmetric matrix  $B \in \mathfrak{so}(n)$  generates a rotation restricted to a single 2-dimensional plane, the matrix exponential in (3) reduces to a finite closed-form expression—mirroring the simplicity of the classic Rodrigues formula for axis-angle rotations [Goldstein et al.,

---

**Algorithm 1** Differentiable Inv. Decomp.

---

**Require:**  $b \in \text{Cl}^2(n)$ ,  $v \in \text{Cl}^1(n)^{k-1}$   
**Ensure:** Inv. Decomp.  $\{b_1, \dots, b_k\}$ ,  
singular vectors  $\{v_1, \dots, v_{k-1}\}$   
1: Initialize **decomp**, **vectors**  $\leftarrow \emptyset, \emptyset$   
2: **for**  $i = 1$  to  $k-1$  **do**  
3:    $b_s, v_i \leftarrow \text{Proj}_{\text{simple}}(b, v_i)$   
4:    $b \leftarrow b - b_s$   
5:   **decomp**  $\leftarrow \text{decomp} \cup \{b_s\}$   
6:   **vectors**  $\leftarrow \text{vectors} \cup \{v_i\}$   
7: **end for**  
8: **decomp**  $\leftarrow \text{decomp} \cup \{b\}$   
9: **return** **decomp**, **vectors**

---

**Algorithm 2** GA Power Iteration

---

**Require:**  $b \in \text{Cl}^2(n)$ ,  $v \in \text{Cl}^1(n)$ ,  
threshold  $\epsilon \in \mathbb{R}$   
**Ensure:** Approximate  $\text{Proj}_{\text{simple}}(b)$   
1:  $v_{\text{prev}} \leftarrow v$   
2: **while**  $\|v + v_{\text{prev}}\| > \epsilon$  **do**  
3:    $v_{\text{prev}} \leftarrow v$   
4:    $v \leftarrow b \llcorner (b \llcorner v)$   
5:    $v \leftarrow v / \|v\|_2$   
6: **end while**  
7:  $\sigma u = b \llcorner v$   
8:  $b_s \leftarrow \sigma u \wedge v$   
9: **return**  $b_s, v$

---

2002]. An analogous simplification holds for bivectors. The exponential map in (4) admits a closed form when  $b \in \text{Cl}^2(n)$  is *simple*, meaning it can be written as  $b = u \wedge v$  for some vectors  $u, v \in \text{Cl}^1(n)$ , or equivalently  $b \wedge b = 0$ . This ensures that  $b$  represents a single-plane rotation rather than a composition of rotations. The resulting closed-form expression is:

$$\exp(b) = \cos(\|b\|) + \frac{\sin(\|b\|)}{\|b\|} b. \quad (5)$$

This form is exact. However, restricting to simple bivectors is limiting, as simple bivectors span only a *subset* of  $\text{Cl}^2(n)$ , and thus generate only a *subset* of  $\text{Spin}(n)$ . To capture the full expressivity of rotor-based transformations, we wish to extend to general bivectors.

**Building bivectors from simple bivectors.** To utilize the closed-form exponential in (5) while retaining the full richness of  $\text{Cl}^2(n)$ , we need a way to express arbitrary bivectors in terms of simple ones. Fortunately, Roelfs and Keninck [2021] show that any bivector  $b \in \text{Cl}^2(n)$  admits an *invariant decomposition* as a sum of at most  $k \triangleq \lfloor n/2 \rfloor$  mutually commuting, orthogonal, simple bivectors  $\{b_1, b_2, \dots, b_k\}$ . This decomposition has two key advantages: (1) each component  $b_i$  admits an efficient closed-form solution  $\exp(b_i)$  in (5) since  $b_i$  is simple, and (2) mutual commutativity ensures  $\exp\left(\sum_{i=1}^k b_i\right) = \prod_{i=1}^k \exp(b_i)$ , via the standard Lie algebra identity  $\exp(X + Y) = \exp(X) \exp(Y)$  when their commutator  $[X, Y] = 0$ . In  $\mathfrak{so}(n)$ , the Lie bracket is  $[X, Y] = XY - YX$ , which vanishes when  $X$  and  $Y$  commute. With these benefits in place, the remaining question is how to construct the decomposition? A recent result provides a spectral formulation in terms of the eigenvectors and eigenvalues of  $b$ , stated below.

**Lemma 2** (Thm. 4.8 in Eelbode et al. [2024]). *Let  $b \in \text{Cl}^2(n)$  have as many eigenvectors as its effective pseudo-dimension. Then, we have*

$$b = \sum_{j=1}^k \mu_j \frac{v_{\mu_j^+} \wedge v_{\mu_j^-}}{v_{\mu_j^+} \cdot v_{\mu_j^-}},$$

where  $\sigma(b) = \{\pm \mu_1, \dots, \mu_k\}$  is the spectrum of  $b$  and  $v_{\mu_j^+}$  and  $v_{\mu_j^-}$  are partner eigenvectors.

**Differentiable invariant decomposition.** While the invariant decomposition can be computed using eigendecomposition, standard algorithms pose challenges. The eigenvalues of a bivector come in conjugate pairs, and singular values come in positive pairs, making differentiation (and backpropagation) not as straightforward due to the numerical instability of eigen-decomposition for near-degenerate singular values. To address this, we introduce a Krylov subspace-inspired algorithm that iteratively extracts the simple bivectors without requiring explicit eigendecomposition. The procedure is shown in Alg. 1. It includes a subroutine for projecting a bivector onto the manifold of simple bivectors, which we accomplish with a Clifford algebraic adaptation of the power iteration method shown in Alg. 2. This uses right contraction  $b \llcorner v$ , which extracts the components of  $b$  that lie in the direction of  $v$ , avoiding the need to construct explicit matrix representations.

The projection has the closed-form expression  $\text{Proj}_{\text{simple}}(b) = \sigma(u \wedge v)$  where  $\sigma$  is the top singular value of  $b$ , and  $u, v$  are the corresponding left and right singular vectors. Note that because of sign symmetry of the paired singular vectors, we detect convergence by the sum, not their difference, and threshold  $\epsilon$ . Further discussion and proofs of Alg.1 –2 are in Appendix B. We provide a full visualization of bivector to rotor in Fig. 3.

**Computation graph size.** To control the size of the computation graph, we adapt DEQ [Bai et al., 2019]: we run the fixed-point iteration without gradient tracking, and then perform a single final forward pass with tracking enabled. This ensures that the graph scales only with  $k$  (number of components in decomposition), and not the number of iterations in Alg. 2, which depends on the spectral gap and threshold  $\epsilon$ . Also, while one could initialize  $v$  in Alg. 2 using a non-differentiable SVD, this is unnecessary. Under small perturbations of  $b$ , the singular vectors vary smoothly. This follows from matrix perturbation results, which guarantees that in non-degenerate cases, eigenspaces vary analytically with the matrix entries (Ch. 2 of Kato [1980]). Thus, warm-starting with the previous singular vectors yields fast convergence, if gradient steps are not too large.

## 4.2 A Generalized Rotor Gadget

Occasionally, we may need mappings between arbitrary dimensional spaces. To do so, we now describe a generalized rotor gadget. Instead of the standard sandwich product in (2), we can allow two different rotors on left/right for more expressiveness. Define the rotor-based transformation as:

$$\psi_{r,s}(x) \triangleq rxs^\dagger, \quad (6)$$

where  $r, s \in \text{Spin}(n)$ . This construction, however, assumes the linear map acts on data with dimension of the Clifford algebra, a power of 2. To address this, we use multiple rotor-sandwich modules operating on different subspaces. For arbitrary input and output dimensions  $d_{\text{in}}$  and  $d_{\text{out}}$ , we utilize the rotor-sandwich modules  $\psi_{r,s}(x)$  as building blocks to construct a map  $\psi : \mathbb{R}^{d_{\text{in}}} \rightarrow \mathbb{R}^{d_{\text{out}}}$ . Fix positive integers  $c_1, c_2$ , and  $n$  with  $2^n \leq \min(d_{\text{in}}, d_{\text{out}})$  and let  $[h] \triangleq \{1, 2, \dots, h\}$ . For each  $i \in [c_1]$  and  $j \in [c_2]$ , define  $I_i \subseteq [d_{\text{in}}]$  and  $O_j \subseteq [d_{\text{out}}]$  as  $2^n$  subsets of input and output coordinates, respectively. We associate each pair with a rotor map  $\psi_{r_{ij}, s_{ij}}$  defined by rotors  $r_{ij}, s_{ij} \in \text{Spin}(n)$ , parametrized by their corresponding bivectors  $a_{ij}, b_{ij} \in \text{Cl}^2(n)$ . Then, each sub-module operates on  $\text{Cl}(n)$  and computes the rotor-sandwich action  $\psi_{r_{ij}, s_{ij}} : \mathbb{R}^{I_i} \rightarrow \mathbb{R}^{O_j}$ . The full output is defined by aggregating all  $c_1 c_2$  rotor maps:

$$\psi(x) \triangleq \sigma(\{\psi_{r_{ij}, s_{ij}}(x^{I_i}) \mid i \in [c_1], j \in [c_2]\}), \quad (7)$$

where  $\sigma$  is a pooling operator on the outputs of  $\psi_{r_{ij}, s_{ij}}$ . Note that  $\bigcup_i I_i = [d_{\text{in}}]$  and  $\bigcup_j O_j = [d_{\text{out}}]$  is needed to fully cover the input and output dimensions. This gives us a general rotor-based transformation from arbitrary input and output dimensions parametrized by bivectors which is visualized in Fig. 4. We now analyze the number of learnable parameters  $\psi$  requires.

**Theorem 1** ( $\psi$  Parameter Count). *Let  $\psi : \mathbb{R}^{d_{\text{in}}} \rightarrow \mathbb{R}^{d_{\text{out}}}$  be the mapping defined above, composed of rotor modules  $\psi_{r_{ij}, s_{ij}}$  with  $i \in [c_1]$  and  $j \in [c_2]$ , each acting in  $\text{Cl}(n)$  with  $2^n \leq \min(d_{\text{in}}, d_{\text{out}}) \triangleq d$ . The total number of learnable parameters is upper bounded by*

$$2c_1 c_2 \binom{n}{2} = \mathcal{O}(\log^2 d).$$

Thm. 1 shows that rotor maps use only  $\mathcal{O}(\log^2 \min(d_{\text{in}}, d_{\text{out}}))$  parameters. In comparison, a standard dense layer and rank- $r$  factorization require  $\mathcal{O}(d_{\text{in}} d_{\text{out}})$  and  $\mathcal{O}(r(d_{\text{in}} + d_{\text{out}}))$ , respectively.

## 5 Experiments

**Goals.** We empirically evaluate rotors by *replacing key, query, and value linear layers in pre-trained LLMs* and measuring downstream performance on perplexity (PPL) and accuracy. Our

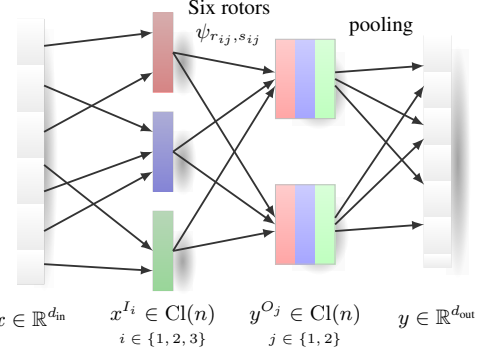


**Figure 4:** Rotor architecture with  $c_1 = 3$  and  $c_2 = 2$ . An input  $x$  is split into  $\{x^{I_i}\}_{i \in [c_1]}$ , each mapped to  $y^{O_j}$  via rotor maps  $\psi_{r_{ij}, s_{ij}}$ , for each  $j \in [c_2]$ . The outputs  $\{y^{O_j}\}$  are pooled and assembled into the final output  $y$ .

input  $x \in \mathbb{R}^{d_{\text{in}}}$  is split into  $x^{I_i} \in \text{Cl}(n)$  for  $i \in [c_1]$ , each mapped to  $y^{O_j} \in \text{Cl}(n)$  for  $j \in [c_2]$ . The outputs  $\{y^{O_j}\}$  are pooled and assembled into the final output  $y$ .

Figure 4 shows the Rotor architecture. An input vector  $x \in \mathbb{R}^{d_{\text{in}}}$  is split into subspaces  $x^{I_i} \in \text{Cl}(n)$  for  $i \in [c_1]$ . Each  $x^{I_i}$  is mapped by a rotor  $\psi_{r_{ij}, s_{ij}}$  to an output  $y^{O_j} \in \text{Cl}(n)$  for  $j \in [c_2]$ . The outputs  $y^{O_j}$  are then pooled and assembled into the final output  $y \in \mathbb{R}^{d_{\text{out}}}$ . The architecture is labeled "Six rotors" and "pooling".

Figure 4 shows the Rotor architecture. An input vector  $x \in \mathbb{R}^{d_{\text{in}}}$  is split into subspaces  $x^{I_i} \in \text{Cl}(n)$  for  $i \in [c_1]$ . Each  $x^{I_i}$  is mapped by a rotor  $\psi_{r_{ij}, s_{ij}}$  to an output  $y^{O_j} \in \text{Cl}(n)$  for  $j \in [c_2]$ . The outputs  $y^{O_j}$  are then pooled and assembled into the final output  $y \in \mathbb{R}^{d_{\text{out}}}$ . The architecture is labeled "Six rotors" and "pooling".

Figure 4 shows the Rotor architecture. An input vector  $x \in \mathbb{R}^{d_{\text{in}}}$  is split into subspaces  $x^{I_i} \in \text{Cl}(n)$  for  $i \in [c_1]$ . Each  $x^{I_i}$  is mapped by a rotor  $\psi_{r_{ij}, s_{ij}}$  to an output  $y^{O_j} \in \text{Cl}(n)$  for  $j \in [c_2]$ . The outputs  $y^{O_j}$  are then pooled and assembled into the final output  $y \in \mathbb{R}^{d_{\text{out}}}$ . The architecture is labeled "Six rotors" and "pooling".

Figure 4 shows the Rotor architecture. An input vector  $x \in \mathbb{R}^{d_{\text{in}}}$  is split into subspaces  $x^{I_i} \in \text{Cl}(n)$  for  $i \in [c_1]$ . Each  $x^{I_i}$  is mapped by a rotor  $\psi_{r_{ij}, s_{ij}}$  to an output  $y^{O_j} \in \text{Cl}(n)$  for  $j \in [c_2]$ . The outputs  $y^{O_j}$  are then pooled and assembled into the final output  $y \in \mathbb{R}^{d_{\text{out}}}$ . The architecture is labeled "Six rotors" and "pooling".

Figure 4 shows the Rotor architecture. An input vector  $x \in \mathbb{R}^{d_{\text{in}}}$  is split into subspaces  $x^{I_i} \in \text{Cl}(n)$  for  $i \in [c_1]$ . Each  $x^{I_i}$  is mapped by a rotor  $\psi_{r_{ij}, s_{ij}}$  to an output  $y^{O_j} \in \text{Cl}(n)$  for  $j \in [c_2]$ . The outputs  $y^{O_j}$  are then pooled and assembled into the final output  $y \in \mathbb{R}^{d_{\text{out}}}$ . The architecture is labeled "Six rotors" and "pooling".

Figure 4 shows the Rotor architecture. An input vector  $x \in \mathbb{R}^{d_{\text{in}}}$  is split into subspaces  $x^{I_i} \in \text{Cl}(n)$  for  $i \in [c_1]$ . Each  $x^{I_i}$  is mapped by a rotor  $\psi_{r_{ij}, s_{ij}}$  to an output  $y^{O_j} \in \text{Cl}(n)$  for  $j \in [c_2]$ . The outputs  $y^{O_j}$  are then pooled and assembled into the final output  $y \in \mathbb{R}^{d_{\text{out}}}$ . The architecture is labeled "Six rotors" and "pooling".

Figure 4 shows the Rotor architecture. An input vector  $x \in \mathbb{R}^{d_{\text{in}}}$  is split into subspaces  $x^{I_i} \in \text{Cl}(n)$  for  $i \in [c_1]$ . Each  $x^{I_i}$  is mapped by a rotor  $\psi_{r_{ij}, s_{ij}}$  to an output  $y^{O_j} \in \text{Cl}(n)$  for  $j \in [c_2]$ . The outputs  $y^{O_j}$  are then pooled and assembled into the final output  $y \in \mathbb{R}^{d_{\text{out}}}$ . The architecture is labeled "Six rotors" and "pooling".

Figure 4 shows the Rotor architecture. An input vector  $x \in \mathbb{R}^{d_{\text{in}}}$  is split into subspaces  $x^{I_i} \in \text{Cl}(n)$  for  $i \in [c_1]$ . Each  $x^{I_i}$  is mapped by a rotor  $\psi_{r_{ij}, s_{ij}}$  to an output  $y^{O_j} \in \text{Cl}(n)$  for  $j \in [c_2]$ . The outputs  $y^{O_j}$  are then pooled and assembled into the final output  $y \in \mathbb{R}^{d_{\text{out}}}$ . The architecture is labeled "Six rotors" and "pooling".

Figure 4 shows the Rotor architecture. An input vector  $x \in \mathbb{R}^{d_{\text{in}}}$  is split into subspaces  $x^{I_i} \in \text{Cl}(n)$  for  $i \in [c_1]$ . Each  $x^{I_i}$  is mapped by a rotor  $\psi_{r_{ij}, s_{ij}}$  to an output  $y^{O_j} \in \text{Cl}(n)$  for  $j \in [c_2]$ . The outputs  $y^{O_j}$  are then pooled and assembled into the final output  $y \in \mathbb{R}^{d_{\text{out}}}$ . The architecture is labeled "Six rotors" and "pooling".

Figure 4 shows the Rotor architecture. An input vector  $x \in \mathbb{R}^{d_{\text{in}}}$  is split into subspaces  $x^{I_i} \in \text{Cl}(n)$  for  $i \in [c_1]$ . Each  $x^{I_i}$  is mapped by a rotor  $\psi_{r_{ij}, s_{ij}}$  to an output  $y^{O_j} \in \text{Cl}(n)$  for  $j \in [c_2]$ . The outputs  $y^{O_j}$  are then pooled and assembled into the final output  $y \in \mathbb{R}^{d_{\text{out}}}$ . The architecture is labeled "Six rotors" and "pooling".

Figure 4 shows the Rotor architecture. An input vector  $x \in \mathbb{R}^{d_{\text{in}}}$  is split into subspaces  $x^{I_i} \in \text{Cl}(n)$  for  $i \in [c_1]$ . Each  $x^{I_i}$  is mapped by a rotor  $\psi_{r_{ij}, s_{ij}}$  to an output  $y^{O_j} \in \text{Cl}(n)$  for  $j \in [c_2]$ . The outputs  $y^{O_j}$  are then pooled and assembled into the final output  $y \in \mathbb{R}^{d_{\text{out}}}$ . The architecture is labeled "Six rotors" and "pooling".

Figure 4 shows the Rotor architecture. An input vector  $x \in \mathbb{R}^{d_{\text{in}}}$  is split into subspaces  $x^{I_i} \in \text{Cl}(n)$  for  $i \in [c_1]$ . Each  $x^{I_i}$  is mapped by a rotor  $\psi_{r_{ij}, s_{ij}}$  to an output  $y^{O_j} \in \text{Cl}(n)$  for  $j \in [c_2]$ . The outputs  $y^{O_j}$  are then pooled and assembled into the final output  $y \in \mathbb{R}^{d_{\text{out}}}$ . The architecture is labeled "Six rotors" and "pooling".

Figure 4 shows the Rotor architecture. An input vector  $x \in \mathbb{R}^{d_{\text{in}}}$  is split into subspaces  $x^{I_i} \in \text{Cl}(n)$  for  $i \in [c_1]$ . Each  $x^{I_i}$  is mapped by a rotor  $\psi_{r_{ij}, s_{ij}}$  to an output  $y^{O_j} \in \text{Cl}(n)$  for  $j \in [c_2]$ . The outputs  $y^{O_j}$  are then pooled and assembled into the final output  $y \in \mathbb{R}^{d_{\text{out}}}$ . The architecture is labeled "Six rotors" and "pooling".

Figure 4 shows the Rotor architecture. An input vector  $x \in \mathbb{R}^{d_{\text{in}}}$  is split into subspaces  $x^{I_i} \in \text{Cl}(n)$  for  $i \in [c_1]$ . Each  $x^{I_i}$  is mapped by a rotor  $\psi_{r_{ij}, s_{ij}}$  to an output  $y^{O_j} \in \text{Cl}(n)$  for  $j \in [c_2]$ . The outputs  $y^{O_j}$  are then pooled and assembled into the final output  $y \in \mathbb{R}^{d_{\text{out}}}$ . The architecture is labeled "Six rotors" and "pooling".

Figure 4 shows the Rotor architecture. An input vector  $x \in \mathbb{R}^{d_{\text{in}}}$  is split into subspaces  $x^{I_i} \in \text{Cl}(n)$  for  $i \in [c_1]$ . Each  $x^{I_i}$  is mapped by a rotor  $\psi_{r_{ij}, s_{ij}}$  to an output  $y^{O_j} \in \text{Cl}(n)$  for  $j \in [c_2]$ . The outputs  $y^{O_j}$  are then pooled and assembled into the final output  $y \in \mathbb{R}^{d_{\text{out}}}$ . The architecture is labeled "Six rotors" and "pooling".

Figure 4 shows the Rotor architecture. An input vector  $x \in \mathbb{R}^{d_{\text{in}}}$  is split into subspaces  $x^{I_i} \in \text{Cl}(n)$  for  $i \in [c_1]$ . Each  $x^{I_i}$  is mapped by a rotor  $\psi_{r_{ij}, s_{ij}}$  to an output  $y^{O_j} \in \text{Cl}(n)$  for  $j \in [c_2]$ . The outputs  $y^{O_j}$  are then pooled and assembled into the final output  $y \in \mathbb{R}^{d_{\text{out}}}$ . The architecture is labeled "Six rotors" and "pooling".

Figure 4 shows the Rotor architecture. An input vector  $x \in \mathbb{R}^{d_{\text{in}}}$  is split into subspaces  $x^{I_i} \in \text{Cl}(n)$  for  $i \in [c_1]$ . Each  $x^{I_i}$  is mapped by a rotor  $\psi_{r_{ij}, s_{ij}}$  to an output  $y^{O_j} \in \text{Cl}(n)$  for  $j \in [c_2]$ . The outputs  $y^{O_j}$  are then pooled and assembled into the final output  $y \in \mathbb{R}^{d_{\text{out}}}$ . The architecture is labeled "Six rotors" and "pooling".

Figure 4 shows the Rotor architecture. An input vector  $x \in \mathbb{R}^{d_{\text{in}}}$  is split into subspaces  $x^{I_i} \in \text{Cl}(n)$  for  $i \in [c_1]$ . Each  $x^{I_i}$  is mapped by a rotor  $\psi_{r_{ij}, s_{ij}}$  to an output  $y^{O_j} \in \text{Cl}(n)$  for  $j \in [c_2]$ . The outputs  $y^{O_j}$  are then pooled and assembled into the final output  $y \in \mathbb{R}^{d_{\text{out}}}$ . The architecture is labeled "Six rotors" and "pooling".

Figure 4 shows the Rotor architecture. An input vector  $x \in \mathbb{R}^{d_{\text{in}}}$  is split into subspaces  $x^{I_i} \in \text{Cl}(n)$  for  $i \in [c_1]$ . Each  $x^{I_i}$  is mapped by a rotor  $\psi_{r_{ij}, s_{ij}}$  to an output  $y^{O_j} \in \text{Cl}(n)$  for  $j \in [c_2]$ . The outputs  $y^{O_j}$  are then pooled and assembled into the final output  $y \in \mathbb{R}^{d_{\text{out}}}$ . The architecture is labeled "Six rotors" and "pooling".

Figure 4 shows the Rotor architecture. An input vector  $x \in \mathbb{R}^{d_{\text{in}}}$  is split into subspaces  $x^{I_i} \in \text{Cl}(n)$  for  $i \in [c_1]$ . Each  $x^{I_i}$  is mapped by a rotor  $\psi_{r_{ij}, s_{ij}}$  to an output  $y^{O_j} \in \text{Cl}(n)$  for  $j \in [c_2]$ . The outputs  $y^{O_j}$  are then pooled and assembled into the final output  $y \in \mathbb{R}^{d_{\text{out}}}$ . The architecture is labeled "Six rotors" and "pooling".

Figure 4 shows the Rotor architecture. An input vector  $x \in \mathbb{R}^{d_{\text{in}}}$  is split into subspaces  $x^{I_i} \in \text{Cl}(n)$  for  $i \in [c_1]$ . Each  $x^{I_i}$  is mapped by a rotor  $\psi_{r_{ij}, s_{ij}}$  to an output  $y^{O_j} \in \text{Cl}(n)$  for  $j \in [c_2]$ . The outputs  $y^{O_j}$  are then pooled and assembled into the final output  $y \in \mathbb{R}^{d_{\text{out}}}$ . The architecture is labeled "Six rotors" and "pooling".

Figure 4 shows the Rotor architecture. An input vector  $x \in \mathbb{R}^{d_{\text{in}}}$  is split into subspaces  $x^{I_i} \in \text{Cl}(n)$  for  $i \in [c_1]$ . Each  $x^{I_i}$  is mapped by a rotor  $\psi_{r_{ij}, s_{ij}}$  to an output  $y^{O_j} \in \text{Cl}(n)$  for  $j \in [c_2]$ . The outputs  $y^{O_j}$  are then pooled and assembled into the final output  $y \in \mathbb{R}^{d_{\text{out}}}$ . The architecture is labeled "Six rotors" and "pooling".

Figure 4 shows the Rotor architecture. An input vector  $x \in \mathbb{R}^{d_{\text{in}}}$  is split into subspaces  $x^{I_i} \in \text{Cl}(n)$  for  $i \in [c_1]$ . Each  $x^{I_i}$  is mapped by a rotor  $\psi_{r_{ij}, s_{ij}}$  to an output  $y^{O_j} \in \text{Cl}(n)$  for  $j \in [c_2]$ . The outputs  $y^{O_j}$  are then pooled and assembled into the final output  $y \in \mathbb{R}^{d_{\text{out}}}$ . The architecture is labeled "Six rotors" and "pooling".

Figure 4 shows the Rotor architecture. An input vector  $x \in \mathbb{R}^{d_{\text{in}}}$  is split into subspaces  $x^{I_i} \in \text{Cl}(n)$  for  $i \in [c_1]$ . Each  $x^{I_i}$  is mapped by a rotor  $\psi_{r_{ij}, s_{ij}}$  to an output  $y^{O_j} \in \text{Cl}(n)$  for  $j \in [c_2]$ . The outputs  $y^{O_j}$  are then pooled and assembled into the final output  $y \in \mathbb{R}^{d_{\text{out}}}$ . The architecture is labeled "Six rotors" and "pooling".

Figure 4 shows the Rotor architecture. An input vector  $x \in \mathbb{R}^{d_{\text{in}}}$  is split into subspaces  $x^{I_i} \in \text{Cl}(n)$  for  $i \in [c_1]$ . Each  $x^{I_i}$  is mapped by a rotor  $\psi_{r_{ij}, s_{ij}}$  to an output  $y^{O_j} \in \text{Cl}(n)$  for  $j \in [c_2]$ . The outputs  $y^{O_j}$  are then pooled and assembled into the final output  $y \in \mathbb{R}^{d_{\text{out}}}$ . The architecture is labeled "Six rotors" and "pooling".

Figure 4 shows the Rotor architecture. An input vector  $x \in \mathbb{R}^{d_{\text{in}}}$  is split into subspaces  $x^{I_i} \in \text{Cl}(n)$  for  $i \in [c_1]$ . Each  $x^{I_i}$  is mapped by a rotor  $\psi_{r_{ij}, s_{ij}}$  to an output  $y^{O_j} \in \text{Cl}(n)$  for  $j \in [c_2]$ . The outputs  $y^{O_j}$  are then pooled and assembled into the final output  $y \in \mathbb{R}^{d_{\text{out}}}$ . The architecture is labeled "Six rotors" and "pooling".

Figure 4 shows the Rotor architecture. An input vector  $x \in \mathbb{R}^{d_{\text{in}}}$  is split into subspaces  $x^{I_i} \in \text{Cl}(n)$  for  $i \in [c_1]$ . Each  $x^{I_i}$  is mapped by a rotor  $\psi_{r_{ij}, s_{ij}}$  to an output  $y^{O_j} \in \text{Cl}(n)$  for  $j \in [c_2]$ . The outputs  $y^{O_j}$  are then pooled and assembled into the final output  $y \in \mathbb{R}^{d_{\text{out}}}$ . The architecture is labeled "Six rotors" and "pooling".

Figure 4 shows the Rotor architecture. An input vector  $x \in \mathbb{R}^{d_{\text{in}}}$  is split into subspaces  $x^{I_i} \in \text{Cl}(n)$  for  $i \in [c_1]$ . Each  $x^{I_i}$  is mapped by a rotor  $\psi_{r_{ij}, s_{ij}}$  to an output  $y^{O_j} \in \text{Cl}(n)$  for  $j \in [c_2]$ . The outputs  $y^{O_j}$  are then pooled and assembled into the final output  $y \in \mathbb{R}^{d_{\text{out}}}$ . The architecture is labeled "Six rotors" and "pooling".

Figure 4 shows the Rotor architecture. An input vector  $x \in \mathbb{R}^{d_{\text{in}}}$  is split into subspaces  $x^{I_i} \in \text{Cl}(n)$  for  $i \in [c_1]$ . Each  $x^{I_i}$  is mapped by a rotor  $\psi_{r_{ij}, s_{ij}}$  to an output  $y^{O_j} \in \text{Cl}(n)$  for  $j \in [c_2]$ . The outputs  $y^{O_j}$  are then pooled and assembled into the final output  $y \in \mathbb{R}^{d_{\text{out}}}$ . The architecture is labeled "Six rotors" and "pooling".

Figure 4 shows the Rotor architecture. An input vector  $x \in \mathbb{R}^{d_{\text{in}}}$  is split into subspaces  $x^{I_i} \in \text{Cl}(n)$  for  $i \in [c_1]$ . Each  $x^{I_i}$  is mapped by a rotor  $\psi_{r_{ij}, s_{ij}}$  to an output  $y^{O_j} \in \text{Cl}(n)$  for  $j \in [c_2]$ . The outputs  $y^{O_j}$  are then pooled and assembled into the final output  $y \in \mathbb{R}^{d_{\text{out}}}$ . The architecture is labeled "Six rotors" and "pooling".

Figure 4 shows the Rotor architecture. An input vector  $x \in \mathbb{R}^{d_{\text{in}}}$  is split into subspaces  $x^{I_i} \in \text{Cl}(n)$  for  $i \in [c_1]$ . Each  $x^{I_i}$  is mapped by a rotor  $\psi_{r_{ij}, s_{ij}}$  to an output  $y^{O_j} \in \text{Cl}(n)$  for  $j \in [c_2]$ . The outputs  $y^{O_j}$  are then pooled and assembled into the final output  $y \in \mathbb{R}^{d_{\text{out}}}$ . The architecture is labeled "Six rotors" and "pooling".

Figure 4 shows the Rotor architecture. An input vector  $x \in \mathbb{R}^{d_{\text{in}}}$  is split into subspaces  $x^{I_i} \in \text{Cl}(n)$  for  $i \in [c_1]$ . Each  $x^{I_i}$  is mapped by a rotor  $\psi_{r_{ij}, s_{ij}}$  to an output  $y^{O_j} \in \text{Cl}(n)$  for  $j \in [c_2]$ . The outputs  $y^{O_j}$  are then pooled and assembled into the final output  $y \in \mathbb{R}^{d_{\text{out}}}$ . The architecture is labeled "Six rotors" and "pooling".

Figure 4 shows the Rotor architecture. An input vector  $x \in \mathbb{R}^{d_{\text{in}}}$  is split into subspaces  $x^{I_i} \in \text{Cl}(n)$  for  $i \in [c_1]$ . Each  $x^{I_i}$  is mapped by a rotor  $\psi_{r_{ij}, s_{ij}}$  to an output  $y^{O_j} \in \text{Cl}(n)$  for  $j \in [c_2]$ . The outputs  $y^{O_j}$  are then pooled and assembled into the final output  $y \in \mathbb{R}^{d_{\text{out}}}$ . The architecture is labeled "Six rotors" and "pooling".

Figure 4 shows the Rotor architecture. An input vector  $x \in \mathbb{R}^{d_{\text{in}}}$  is split into subspaces  $x^{I_i} \in \text{Cl}(n)$  for  $i \in [c_1]$ . Each  $x^{I_i}$  is mapped by a rotor  $\psi_{r_{ij}, s_{ij}}$  to an output  $y^{O_j} \in \text{Cl}(n)$  for  $j \in [c_2]$ . The outputs  $y^{O_j}$  are then pooled and assembled into the final output  $y \in \mathbb{R}^{d_{\text{out}}}$ . The architecture is labeled "Six rotors" and "pooling".

Figure 4 shows the Rotor architecture. An input vector  $x \in \mathbb{R}^{d_{\text{in}}}$  is split into subspaces  $x^{I_i} \in \text{Cl}(n)$  for  $i \in [c_1]$ . Each  $x^{I_i}$  is mapped by a rotor  $\psi_{r_{ij}, s_{ij}}$  to an output  $y^{O_j} \in \text{Cl}(n)$  for  $j \in [c_2]$ . The outputs  $y^{O_j}$  are then pooled and assembled into the final output  $y \in \mathbb{R}^{d_{\text{out}}}$ . The architecture is labeled "Six rotors" and "pooling".

Figure 4 shows the Rotor architecture. An input vector  $x \in \mathbb{R}^{d_{\text{in}}}$  is split into subspaces  $x^{I_i} \in \text{Cl}(n)$  for  $i \in [c_1]$ . Each  $x^{I_i}$  is mapped by a rotor  $\psi_{r_{ij}, s_{ij}}$  to an output  $y^{O_j} \in \text{Cl}(n)$  for  $j \in [c_2]$ . The outputs  $y^{O_j}$  are then pooled and assembled into the final output  $y \in \mathbb{R}^{d_{\text{out}}}$ . The architecture is labeled "Six rotors" and "pooling".

Figure 4 shows the Rotor architecture. An input vector  $x \in \mathbb{R}^{d_{\text{in}}}$  is split into subspaces  $x^{I_i} \in \text{Cl}(n)$  for  $i \in [c_1]$ . Each  $x^{I_i}$  is mapped by a rotor  $\psi_{r_{ij}, s_{ij}}$  to an output  $y^{O_j} \in \text{Cl}(n)$  for  $j \in [c_2]$ . The outputs  $y^{O_j}$  are then pooled and assembled into the final output  $y \in \mathbb{R}^{d_{\text{out}}}$ . The architecture is labeled "Six rotors" and "pooling".

Figure 4 shows the Rotor architecture. An input vector  $x \in \mathbb{R}^{d_{\text{in}}}$  is split into subspaces  $x^{I_i} \in \text{Cl}(n)$  for  $i \in [c_1]$ . Each  $x^{I_i}$  is mapped by a rotor  $\psi_{r_{ij}, s_{ij}}$  to an output  $y^{O_j} \in \text{Cl}(n)$  for  $j \in [c_2]$ . The outputs  $y^{O_j}$  are then pooled and assembled into the final output  $y \in \mathbb{R}^{d_{\text{out}}}$ . The architecture is labeled "Six rotors" and "pooling".

Figure 4 shows the Rotor architecture. An input vector  $x \in \mathbb{R}^{d_{\text{in}}}$  is split into subspaces  $x^{I_i} \in \text{Cl}(n)$  for  $i \in [c_1]$ . Each  $x^{I_i}$  is mapped by a rotor  $\psi_{r_{ij}, s_{ij}}$  to an output  $y^{O_j} \in \text{Cl}(n)$  for  $j \in [c_2]$ . The outputs  $y^{O_j}$  are then pooled and assembled into the final output  $y \in \mathbb{R}^{d_{\text{out}}}$ . The architecture is labeled "Six rotors" and "pooling".

Figure 4 shows the Rotor architecture. An input vector  $x \in \mathbb{R$

experiments span multiple models and datasets. The main goals are to: **(G-1)** Demonstrate the *feasibility of composing linear layers from bivector primitives* by assessing whether rotors match baseline performance of Low-Rank and Block-Hadamard approximations across diverse settings. **(G-2)** Quantify rotor parameter efficiency compared to dense and approximate alternatives. **(G-3)** Analyze how rotor architectural choices—such as width and depth—affect performance.

We focus on linear layers in smaller pre-trained language models (up to 1.5B parameters), where reduced redundancy compared to larger models makes preserving performance harder. We do not attempt full model conversion—which would require larger calibration datasets and a layerwise optimization scheme like GPTQ [Frantar et al., 2022]. Instead, we selectively replace 1-3 attention layers (key, query, and value projections) to isolate the effect, and assess whether rotor decomposition offers competitive PPL and accuracy relative to baselines.

## 5.1 Experimental Setup

**Substituting attention layers.** Given  $x \in \mathbb{R}^d$  to a transformer block, we have:

$$\text{Attn}(x) = \left[ \text{softmax} \left( \text{mask} \left( \frac{QK^\top}{\sqrt{d}} \right) \right) V \right] W_o,$$

where the query, key, and value linear projections are defined as  $Q = W_q x$ ,  $K = W_k x$ , and  $V = W_v x$ , with  $W_q$ ,  $W_k$ , and  $W_v$  as dense learnable matrices. We *jointly* replace these linear layers in 1-3 selected attention layers with rotors or baseline approximations, *keeping other parameters fixed* except, for consistency, retraining the corresponding output linear layer  $W_o$  after each substitution.

### Training protocol and architectural choices.

To fit each substitute layer (rotor, LR, or BH), we extract hidden states from the pre-trained model and minimize MSE between the projected outputs of the original and approximated layers. Each variant is trained independently using the Adam optimizer [Kingma and Ba, 2017]. In our rotor architecture, *depth* refers to the number of stacked rotor maps  $\psi$ , while *width* denotes the number of parallel rotor maps within each layer. For example, the rotor map in Fig. 4 has both width and depth equal to 1 (i.e., one rotor map). We also insert *fixed permutations* between rotors to enable grade mixing and add *normalization* layers to stabilize training; both are parameter-free. All architectural details and hyperparameters are provided in Appendix C.

| Dataset      | Method        | LLaMA-3.2 1B  |  |  | Qwen-2.5 1.5B                          |  |  |
|--------------|---------------|---------------|--|--|--|--|--|
|              |               | one           | two                                    | three                                  | one                                    | two                                    | three  |
| Log-PPL      | Wikitext2     | Original      | —                                      | 2.575                                  | —                                      | 2.287                                  | —  |
|              |               | LR1           | 2.688                                  | 3.455                                  | 4.956                                  | 2.350                                  | 2.402  |
|              |               | LR4           | 2.658                                  | 2.729                                  | 2.880                                  | 2.342                                  | 2.372 <span style="color:blue;">2.548</span> |
|              |               | BH1           | <span style="color:blue;">2.636</span> | <span style="color:red;">2.700</span>  | <span style="color:red;">2.779</span>  | <span style="color:blue;">2.323</span> | 2.388  |
|              | C4            | Rotor         | <span style="color:blue;">2.629</span> | <span style="color:blue;">2.717</span> | <span style="color:blue;">2.818</span> | <span style="color:blue;">2.307</span> | <span style="color:blue;">2.369</span>       |
|              |               | Original      | —                                      | 3.151                                  | —                                      | 2.834                                  | —  |
|              |               | LR1           | 3.414                                  | 4.071                                  | 5.001                                  | 2.884                                  | 2.910  |
|              |               | LR4           | 3.390                                  | 3.315                                  | 3.504                                  | 2.874                                  | 2.905  |
|              | PTB           | BH1           | <span style="color:blue;">3.343</span> | <span style="color:blue;">3.262</span> | <span style="color:blue;">3.404</span> | <span style="color:blue;">2.865</span> | <span style="color:red;">2.897</span>        |
|              |               | Rotor         | <span style="color:blue;">3.261</span> | <span style="color:blue;">3.285</span> | <span style="color:blue;">3.428</span> | <span style="color:blue;">2.854</span> | <span style="color:blue;">2.900</span>       |
|              |               | Original      | —                                      | 3.260                                  | —                                      | 2.985                                  | —  |
|              |               | LR1           | 3.358                                  | 4.684                                  | 6.904                                  | 3.046                                  | 3.151  |
|              | Accuracy (%)  | LR4           | <span style="color:blue;">3.316</span> | 3.400                                  | 3.466                                  | 3.034                                  | 3.127  |
|              |               | BH1           | <span style="color:blue;">3.293</span> | <span style="color:blue;">3.355</span> | <span style="color:blue;">3.395</span> | <span style="color:blue;">3.025</span> | <span style="color:blue;">3.101</span>       |
|              |               | Rotor         | 3.327                                  | <span style="color:blue;">3.392</span> | <span style="color:blue;">3.442</span> | <span style="color:blue;">3.011</span> | <span style="color:blue;">3.109</span>       |
|              |               | Arc Challenge | Original                               | —                                      | 58.37                                  | —                                      | 66.09  |
| Accuracy (%) | Arc Challenge | LR1           | 50.78                                  | 50.44                                  | 44.26                                  | 55.06                                  | 50.97  |
|              |               | LR4           | 53.84                                  | 53.39                                  | 45.95                                  | 57.48                                  | <span style="color:red;">54.51</span>        |
|              |               | BH1           | <span style="color:blue;">54.83</span> | <span style="color:blue;">54.25</span> | <span style="color:blue;">49.61</span> | <span style="color:blue;">60.11</span> | <span style="color:red;">60.77</span>        |
|              |               | Rotor         | <span style="color:blue;">55.31</span> | <span style="color:blue;">54.50</span> | <span style="color:blue;">49.64</span> | <span style="color:blue;">61.34</span> | <span style="color:blue;">52.27</span>       |
|              | HellaSwag     | Original      | —                                      | 41.00                                  | —                                      | 55.00                                  | —  |
|              |               | LR1           | 36.17                                  | 28.93                                  | 14.47                                  | 42.53                                  | 32.33  |
|              |               | LR4           | 38.02                                  | 33.79                                  | 33.87                                  | 44.41                                  | 40.53  |
|              |               | BH1           | <span style="color:blue;">39.10</span> | <span style="color:red;">35.27</span>  | <span style="color:red;">35.87</span>  | <span style="color:red;">45.96</span>  | <span style="color:red;">42.73</span>        |
|              |               | Rotor         | <span style="color:blue;">39.33</span> | <span style="color:blue;">34.94</span> | <span style="color:blue;">37.52</span> | <span style="color:blue;">50.20</span> | <span style="color:blue;">40.60</span>       |

**Table 1:** Log PPL ( $\downarrow$ ) and accuracy ( $\uparrow$ ) using original, Low-Rank (1 or 4), BH1, and Rotor (ours) for 1-3 layer replacements. One-layer results are averaged over all layers; two/three-layer results are averaged over five random selections. Red indicates best, blue second-best per setting.

### Models, datasets, and baselines.

We evaluate on two pre-trained LLMs: LLaMA-3.2 1B [Touvron et al., 2023] and Qwen-2.5 1.5B [Qwen et al., 2025]. Metrics include log perplexity ( $\downarrow$ ) on three language modeling datasets—Wikitext2, C4 [Dodge et al., 2021], and PTB [Marcus et al., 1993]—and accuracy ( $\uparrow$ ) on two multiple-choice benchmarks—Arc Challenge [Clark et al., 2018] and HellaSwag [Zellers et al., 2019]. We compare our rotors to: **(a) LR1 and LR4:** Low-rank projections with rank  $r = 1$  or 4, where a dense matrix  $W \in \mathbb{R}^{d_{\text{out}} \times d_{\text{in}}}$  is approximated as  $XY$ , with  $X \in \mathbb{R}^{d_{\text{out}} \times r}$  and  $Y \in \mathbb{R}^{r \times d_{\text{in}}}$ . **(b) BH1:** Block-Hadamard [Zeng et al., 2023] of depth 1, which approximate  $W$  by  $BH$ , where  $H$  is a fixed Hadamard matrix and  $B$  is block-diagonal and learnable. Parameter counts for all the methods are detailed in Tab. 3; reference LLM performance (with dense matrices) are shown in Tab. 1. Additional experiments are provided in Appendix D.

| Dataset           | Method | One layer replaced (Layer index)  |       |       |       |       |       |       |       |       |       |       |       |       |       |       |
|-------------------|--------|-----------------------------------|-------|-------|-------|-------|-------|-------|-------|-------|-------|-------|-------|-------|-------|-------|
|                   |        | 1                                 | 2     | 3     | 4     | 5     | 6     | 7     | 8     | 9     | 10    | 11    | 12    | 13    | 14    | 15    |
| Wikitext2 (↓)     | LR1    | 3.620                             | 2.750 | 2.754 | 2.781 | 2.742 | 2.705 | 2.703 | 2.714 | 2.695 | 2.622 | 2.632 | 2.628 | 2.612 | 2.630 | 2.647 |
|                   | LR4    | 3.851                             | 2.723 | 2.752 | 2.673 | 2.673 | 2.650 | 2.671 | 2.667 | 2.674 | 2.620 | 2.628 | 2.614 | 2.602 | 2.620 | 2.634 |
|                   | BH1    | 3.615                             | 2.686 | 2.675 | 2.645 | 2.657 | 2.637 | 2.645 | 2.653 | 2.647 | 2.612 | 2.617 | 2.612 | 2.592 | 2.606 | 2.614 |
|                   | Rotor  | 2.924                             | 2.665 | 2.664 | 2.645 | 2.664 | 2.635 | 2.642 | 2.640 | 2.640 | 2.607 | 2.616 | 2.613 | 2.593 | 2.611 | 2.566 |
| C4 (↓)            | LR1    | 4.433                             | 3.297 | 3.440 | 3.274 | 3.300 | 3.276 | 3.309 | 3.282 | 3.292 | 3.205 | 3.284 | 3.271 | 3.192 | 3.236 | 3.214 |
|                   | LR4    | 4.432                             | 3.292 | 3.404 | 3.250 | 3.266 | 3.250 | 3.264 | 3.260 | 3.281 | 3.203 | 3.204 | 3.191 | 3.187 | 3.219 | 3.208 |
|                   | BH1    | 4.293                             | 3.288 | 3.276 | 3.212 | 3.230 | 3.215 | 3.241 | 3.230 | 3.276 | 3.196 | 3.193 | 3.184 | 3.174 | 3.194 | 3.194 |
|                   | Rotor  | 3.660                             | 3.258 | 3.292 | 3.232 | 3.242 | 3.228 | 3.249 | 3.245 | 3.248 | 3.197 | 3.196 | 3.187 | 3.176 | 3.202 | 3.203 |
| PTB (↓)           | LR1    | 5.401                             | 3.468 | 3.435 | 3.406 | 3.419 | 3.346 | 3.358 | 3.401 | 3.363 | 3.322 | 3.281 | 3.308 | 3.271 | 3.322 | 3.292 |
|                   | LR4    | 5.183                             | 3.394 | 3.395 | 3.316 | 3.347 | 3.304 | 3.315 | 3.334 | 3.328 | 3.281 | 3.276 | 3.265 | 3.264 | 3.308 | 3.287 |
|                   | BH1    | 4.835                             | 3.352 | 3.336 | 3.293 | 3.324 | 3.288 | 3.292 | 3.307 | 3.302 | 3.273 | 3.266 | 3.268 | 3.255 | 3.265 | 3.270 |
|                   | Rotor  | 4.194                             | 3.412 | 3.403 | 3.356 | 3.369 | 3.320 | 3.338 | 3.336 | 3.326 | 3.278 | 3.271 | 3.300 | 3.266 | 3.300 | 3.284 |
| Arc Challenge (↑) | LR1    | 50.64                             | 53.22 | 46.78 | 46.35 | 45.49 | 51.07 | 52.79 | 51.93 | 33.05 | 50.21 | 56.65 | 55.80 | 56.65 | 55.08 | 55.79 |
|                   | LR4    | 50.64                             | 53.22 | 50.64 | 51.93 | 54.51 | 55.79 | 54.08 | 51.07 | 46.35 | 51.07 | 58.80 | 59.23 | 57.51 | 56.22 | 57.51 |
|                   | BH1    | 53.22                             | 54.51 | 52.79 | 54.94 | 57.08 | 54.08 | 53.65 | 52.36 | 51.93 | 50.21 | 57.94 | 57.08 | 58.80 | 57.51 | 57.51 |
|                   | Rotor  | 54.51                             | 55.36 | 53.65 | 55.36 | 54.51 | 55.79 | 54.51 | 53.22 | 52.36 | 50.64 | 58.37 | 60.09 | 56.65 | 57.94 | 57.08 |
| HellaSwag (↑)     | LR1    | 29.00                             | 32.00 | 34.33 | 39.67 | 34.00 | 33.00 | 34.00 | 33.00 | 34.67 | 37.00 | 41.00 | 38.33 | 40.33 | 40.00 | 39.67 |
|                   | LR4    | 32.67                             | 39.67 | 34.67 | 39.00 | 37.67 | 37.00 | 35.00 | 38.67 | 33.67 | 37.67 | 41.33 | 40.00 | 40.33 | 40.33 | 40.00 |
|                   | BH1    | 37.33                             | 37.67 | 37.67 | 41.00 | 37.00 | 40.00 | 40.33 | 37.00 | 36.33 | 36.33 | 42.67 | 40.00 | 41.33 | 42.00 | 41.33 |
|                   | Rotor  | 40.00                             | 39.67 | 35.67 | 42.33 | 41.00 | 38.67 | 36.67 | 38.67 | 36.00 | 36.67 | 42.00 | 39.67 | 40.33 | 42.00 | 40.67 |
| Dataset           | Method | Two layers replaced (Layer pairs) |       |       |       |       |       |       |       |       |       |       |       |       |       |       |
|                   |        | 10,11                             | 10,12 | 10,13 | 10,14 | 10,15 | 11,12 | 11,13 | 11,14 | 11,15 | 12,13 | 12,14 | 12,15 | 13,14 | 13,15 | 14,15 |
| Wikitext2 (↓)     | LR1    | 2.724                             | 2.702 | 2.695 | 2.697 | 2.718 | 2.757 | 2.731 | 2.756 | 2.757 | 2.768 | 2.723 | 2.741 | 2.729 | 2.863 | 2.862 |
|                   | LR4    | 2.703                             | 2.674 | 2.662 | 2.669 | 2.694 | 2.691 | 2.662 | 2.669 | 2.694 | 2.660 | 2.665 | 2.676 | 2.686 | 2.708 | 2.758 |
|                   | BH1    | 2.677                             | 2.660 | 2.645 | 2.650 | 2.656 | 2.670 | 2.643 | 2.662 | 2.660 | 2.645 | 2.656 | 2.657 | 2.655 | 2.680 | 2.700 |
|                   | Rotor  | 2.679                             | 2.670 | 2.654 | 2.660 | 2.676 | 2.662 | 2.652 | 2.667 | 2.677 | 2.667 | 2.675 | 2.675 | 2.662 | 2.688 | 2.745 |
| C4 (↓)            | LR1    | 3.298                             | 3.273 | 3.258 | 3.296 | 3.293 | 3.315 | 3.276 | 3.315 | 3.303 | 3.263 | 3.300 | 3.281 | 3.285 | 3.278 | 3.386 |
|                   | LR4    | 3.290                             | 3.258 | 3.249 | 3.279 | 3.269 | 3.265 | 3.255 | 3.287 | 3.271 | 3.241 | 3.278 | 3.246 | 3.281 | 3.268 | 3.353 |
|                   | BH1    | 3.281                             | 3.241 | 3.228 | 3.246 | 3.244 | 3.242 | 3.227 | 3.246 | 3.244 | 3.216 | 3.237 | 3.226 | 3.234 | 3.232 | 3.296 |
|                   | Rotor  | 3.267                             | 3.246 | 3.231 | 3.256 | 3.254 | 3.248 | 3.232 | 3.260 | 3.257 | 3.223 | 3.252 | 3.241 | 3.249 | 3.247 | 3.327 |
| PTB (↓)           | LR1    | 3.385                             | 3.386 | 3.367 | 3.410 | 3.402 | 3.418 | 3.370 | 3.418 | 3.367 | 3.486 | 3.423 | 3.371 | 3.431 | 3.455 | 3.619 |
|                   | LR4    | 3.345                             | 3.319 | 3.320 | 3.348 | 3.336 | 3.326 | 3.315 | 3.353 | 3.332 | 3.300 | 3.317 | 3.313 | 3.367 | 3.335 | 3.419 |
|                   | BH1    | 3.315                             | 3.307 | 3.297 | 3.304 | 3.310 | 3.309 | 3.287 | 3.332 | 3.301 | 3.281 | 3.293 | 3.298 | 3.294 | 3.300 | 3.345 |
|                   | Rotor  | 3.336                             | 3.343 | 3.311 | 3.349 | 3.334 | 3.339 | 3.303 | 3.342 | 3.299 | 3.311 | 3.359 | 3.336 | 3.352 | 3.342 | 3.441 |
| Arc Challenge (↑) | LR1    | 43.06                             | 46.07 | 46.50 | 48.21 | 43.92 | 46.93 | 55.51 | 57.23 | 55.94 | 52.94 | 54.65 | 54.65 | 54.22 | 55.51 | 54.65 |
|                   | LR4    | 42.92                             | 48.50 | 48.07 | 51.07 | 49.79 | 59.23 | 56.65 | 59.23 | 57.94 | 58.80 | 56.65 | 57.51 | 56.22 | 55.36 | 57.94 |
|                   | BH1    | 43.35                             | 48.50 | 51.07 | 50.21 | 50.64 | 59.66 | 58.37 | 58.80 | 56.65 | 57.94 | 59.23 | 57.51 | 57.94 | 55.65 | 58.37 |
|                   | Rotor  | 45.49                             | 48.93 | 53.65 | 52.79 | 51.50 | 57.94 | 57.94 | 58.80 | 56.65 | 59.66 | 56.65 | 57.08 | 57.03 | 55.79 | 57.05 |
| HellaSwag (↑)     | LR1    | 32.00                             | 35.00 | 36.00 | 40.33 | 34.00 | 37.67 | 41.67 | 39.33 | 41.33 | 34.00 | 40.33 | 39.33 | 40.33 | 43.00 | 40.67 |
|                   | LR4    | 32.33                             | 35.33 | 38.33 | 38.33 | 36.67 | 39.00 | 41.67 | 41.00 | 42.33 | 40.00 | 38.00 | 39.00 | 40.00 | 39.00 | 37.67 |
|                   | BH1    | 37.33                             | 37.67 | 35.67 | 40.33 | 39.33 | 39.33 | 41.00 | 41.67 | 41.33 | 40.33 | 43.67 | 40.67 | 42.67 | 40.67 | 40.67 |
|                   | Rotor  | 36.00                             | 37.67 | 38.67 | 38.67 | 37.67 | 39.33 | 41.67 | 41.33 | 41.33 | 39.33 | 41.67 | 39.00 | 41.00 | 40.33 | 40.33 |

**Table 2:** Performance on Log-PPL (↓) and accuracy (↑) when replacing **one attention layer (top)** for layer indices 1–15 and **two attention layers (bottom)** for pairs of indices from 10–15 of LLaMA-3.2 1B. Methods are Low Rank ( $r = 1$  and 4), BH1, and our Rotor.

## 5.2 Results and Discussion

**Parameter efficiency.** As shown in Tab. 3, rotors require significantly fewer parameters than both dense and approximate baselines. For example, in LLaMA-1B, the query projection uses over 4.19M parameters in its dense form, compared to 16.4K in LR4, 32.7K in BH1, and just  $\leq 896$  in rotors—4700 $\times$  reduction over dense and 18 $\times$  over LR4. Similar savings apply across key and value layers, directly supporting **G-2**.

**Rotor performance vs. baselines.** Despite their compact size, rotors match or outperform LR1, LR4, and BH1 across most datasets and models. In Tab. 1, on Wikitext2, rotors achieve 2.629 log-PPL in LLaMA-1B (vs. 2.636 for second-best BH1), and 2.307 in Qwen-1.5B (vs. 2.323 for second-best BH1) when a single attention layer is replaced. On Arc Challenge, rotor layers yield 55.31% accuracy in LLaMA-1B (vs. 54.83% for BH1) and 61.34% in Qwen-1.5B (vs. 57.48% for LR4). Rotor projections are consistently either the best or second-best across most settings.

Tab. 2 confirms rotor robustness across layer combinations. For example, replacing layers 12 and 13 in Qwen-1.5B yields 59.66% accuracy on Arc Challenge—outperforming LR4 (58.80%) and BH1 (57.94%). In contrast, LR1—despite having 2–5 $\times$  more parameters than rotors—shows significant performance drops (e.g., log-PPL on Wikitext2 for LLaMA-1B). These results confirm **G-1** and show that rotors match downstream performance of other baselines only using far fewer parameters.

In Fig. 5, PPL consistently decreases with both increasing rotor *width* and *depth*. The strongest improvements occur from depth 1 to 2, after which gains taper off. This trend suggests that both stacking more layers (depth) and using more parallel rotor maps (width) contribute to better approximation of linear layers—showing **G-3**.

Overall, our results support our claim: rotor layers—constructed from bivector primitives—offer insight into how linear layers can be synthesized from a compact set of building blocks.

## 6 Related Work

**Compositions in machine learning.** Building complex model behavior from composition of simpler compute primitives is an active research topic. Capsule networks [Sabour et al., 2017] modeled part-whole relations, while mixture-of-experts [Riquelme et al., 2021] and model merging [Lähner and Moeller, 2024] compose specialized sub-modules in a conditional manner. Recent studies show how internal circuits in LLMs organize around functional units [Weiss et al., 2021]. In NLP, Tree-structured models [Tai et al., 2015] have been used to encode syntactic composition, while works on compositional semantics [Mitchell and Lapata, 2008] investigate how word meanings compose to form sentence meanings. The ability to understand new combinations of familiar components remains a challenge [Zhou et al., 2024, Lake and Baroni, 2018] and a few strategies are being studied [Li et al., 2022, Chen et al., 2020, Chytas et al., 2024]. Other directions include modular approaches [Das et al., 2018, Pfeiffer et al., 2023].

**Approximating linear layers.** To reduce the cost of dense layers, various structured approximations are common. Low-rank factorization such as LoRA [Hu et al., 2021] constrains weights to rank- $r$  matrices. Other matrices such as circulant [Yu et al., 2014, Cheng et al., 2015], Toeplitz [Sindhwan et al., 2015], Walsh-Hadamard [Alam et al., 2024], and Block-Hadamard [Zeng et al., 2023], among others, have been shown to be resource efficient. Our goal is to understand the compositional structure of the linear transformation itself. Resource efficiency is the *result*, not the key motivation.

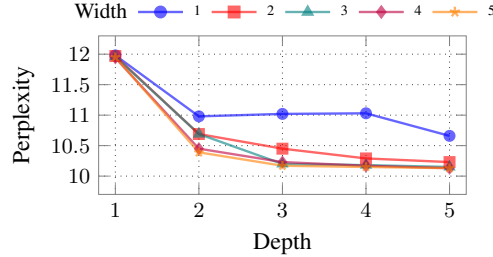


**Figure 5:** Effect of rotor width and depth on Wiki-text2 when replacing layer 13 in Qwen 1.5B.

| Method | Key         | Query      | Value       |
|--------|-------------|------------|-------------|
| Dense  | 1048576     | 4194304    | 1048576     |
| LR1    | 2560        | 4096       | 2560        |
| LR4    | 10240       | 16384      | 10240       |
| BH1    | 8192        | 32768      | 8192        |
| Rotor  | $\leq 1080$ | $\leq 896$ | $\leq 1080$ |

**Table 3:** Summary of the number of parameters used for key, query, and value projections in a single attention layer of LLaMA-3.2 1B.

**Clifford/Geometric algebra in ML.** Recent works have explored Clifford algebra for encoding geometric structure in ML models. GCANs [Ruhe et al., 2023b] and CGENN [Ruhe et al., 2023a] construct equivariant layers by combining GA-based transformations. Clifford neural layers [Brandstetter et al., 2023] was applied to physical modeling tasks. GA has been connected to convex training of ReLU networks [Pilanci, 2024] and randomized methods for multivector representations [Wang et al., 2024] are available. GA has also been used for time-series models [Chen et al., 2025].

## 7 Conclusions

We show that the functionality of standard linear layers can be expressed with exponentially fewer parameters— $\mathcal{O}(\log^2 d)$  versus  $\mathcal{O}(d^2)$ —while maintaining competitive performance when applied to attention mechanisms in modern LLMs. The underlying algebraic structure suggests a rich compositional hierarchy, where geometric primitives combine through rotor operations to produce richer transformations. These conceptual results open several promising directions including the development of interpretable architectures and parameter-efficient models that leverage this compositional structure. Beyond LLMs, our results have connections to statistical models requiring interaction decomposition, such as ANOVA [St et al., 1989], multivariate analysis [Mardia et al., 2024], and mechanisms to approximate Shapley features [Chen et al., 2023].

## References

Samira Abnar, Omid Saremi, Laurent Dinh, Shantel Wilson, Miguel Angel Bautista, Chen Huang, Vimal Thilak, Eta Littwin, Jiatao Gu, Josh Susskind, and Samy Bengio. Adaptivity and modularity for efficient generalization over task complexity, 2023. URL <https://arxiv.org/abs/2310.08866>.

Mohammad Mahmudul Alam, Alexander Oberle, Edward Raff, Stella Biderman, Tim Oates, and James Holt. A walsh hadamard derived linear vector symbolic architecture. *arXiv preprint arXiv:2410.22669*, 2024.

Francesco Alesiani. Pytorch geometric algebra, 2023. URL [https://github.com/falesiani/torch\\_ga](https://github.com/falesiani/torch_ga).

Shaojie Bai, J. Zico Kolter, and Vladlen Koltun. Deep equilibrium models, 2019. URL <https://arxiv.org/abs/1909.01377>.

Johannes Brandstetter, Rianne van den Berg, Max Welling, and Jayesh K. Gupta. Clifford neural layers for pde modeling, 2023. URL <https://arxiv.org/abs/2209.04934>.

Julian Büchel, Athanasios Vasilopoulos, William Andrew Simon, Irem Boybat, HsinYu Tsai, Geofrey W Burr, Hernan Castro, Bill Filipiak, Manuel Le Gallo, Abbas Rahimi, et al. Efficient scaling of large language models with mixture of experts and 3d analog in-memory computing. *Nature Computational Science*, pages 1–14, 2025.

Hui Chen, Viet Luong, Lopamudra Mukherjee, and Vikas Singh. Simpletm: A simple baseline for multivariate time series forecasting. In *The Thirteenth International Conference on Learning Representations*, 2025.

Lu Chen, Siyu Lou, Keyan Zhang, Jin Huang, and Quanshi Zhang. Harsanyinet: Computing accurate shapley values in a single forward propagation. *arXiv preprint arXiv:2304.01811*, 2023.

Xinyun Chen, Chen Liang, Adams Wei Yu, Dawn Song, and Denny Zhou. Compositional generalization via neural-symbolic stack machines. *Advances in Neural Information Processing Systems*, 33: 1690–1701, 2020.

Yu Cheng, Felix X Yu, Rogerio S Feris, Sanjiv Kumar, Alok Choudhary, and Shi-Fu Chang. An exploration of parameter redundancy in deep networks with circulant projections. In *Proceedings of the IEEE international conference on computer vision*, pages 2857–2865, 2015.

Sotirios Panagiotis Chytas, Hyunwoo J Kim, and Vikas Singh. Understanding multi-compositional learning in vision and language models via category theory. In *European Conference on Computer Vision*, pages 324–341. Springer, 2024.

Peter Clark, Isaac Cowhey, Oren Etzioni, Tushar Khot, Ashish Sabharwal, Carissa Schoenick, and Oyvind Tafjord. Think you have solved question answering? try arc, the ai2 reasoning challenge, 2018. URL <https://arxiv.org/abs/1803.05457>.

P. M. Cohn. *Basic Algebra: Groups, Rings and Fields*. Springer, London, 2003. doi: 10.1007/978-0-85729-428-9.

Keith Conrad. Exterior powers. Lecture notes, Department of Mathematics, University of Connecticut, n.d. Available at <https://kconrad.math.uconn.edu/blurbs/linmultialg/extmod.pdf>.

Abhishek Das, Georgia Gkioxari, Stefan Lee, Devi Parikh, and Dhruv Batra. Neural modular control for embodied question answering. In *Conference on robot learning*, pages 53–62. PMLR, 2018.

Jesse Dodge, Maarten Sap, Ana Marasović, William Agnew, Gabriel Ilharco, Dirk Groeneveld, Margaret Mitchell, and Matt Gardner. Documenting large webtext corpora: A case study on the colossal clean crawled corpus, 2021. URL <https://arxiv.org/abs/2104.08758>.

David Eelbode, Martin Roelfs, and Steven De Keninck. Outer and eigen: Tangent concepts, 2024. URL <https://arxiv.org/abs/2412.20566>.

Elias Frantar, Saleh Ashkboos, Torsten Hoefer, and Dan Alistarh. Gptq: Accurate post-training quantization for generative pre-trained transformers. *arXiv preprint arXiv:2210.17323*, 2022.

Badih Ghazi, Rina Panigrahy, and Joshua Wang. Recursive sketches for modular deep learning. In Kamalika Chaudhuri and Ruslan Salakhutdinov, editors, *Proceedings of the 36th International Conference on Machine Learning*, volume 97 of *Proceedings of Machine Learning Research*, pages 2211–2220. PMLR, 09–15 Jun 2019. URL <https://proceedings.mlr.press/v97/ghazi19a.html>.

Herbert Goldstein, Charles P. Poole, and John L. Safko. *Classical Mechanics*. Addison-Wesley, 3rd edition, 2002. ISBN 978-0201657029.

Gene H. Golub and Charles F. Van Loan. *Matrix Computations*. Johns Hopkins University Press, Baltimore, MD, 4th edition, 2013. ISBN 9781421407944.

David Hestenes and Garret Sobczyk. *Clifford algebra to geometric calculus: a unified language for mathematics and physics*, volume 5. Springer Science & Business Media, 2012.

Eckhard Hitzer. Introduction to clifford’s geometric algebra. *arXiv preprint arXiv:1306.1660*, 2013. URL <https://arxiv.org/abs/1306.1660>.

Edward J. Hu, Yelong Shen, Phillip Wallis, Zeyuan Allen-Zhu, Yuanzhi Li, Shean Wang, Lu Wang, and Weizhu Chen. Lora: Low-rank adaptation of large language models, 2021. URL <https://arxiv.org/abs/2106.09685>.

Zijian Hu, Jipeng Zhang, Rui Pan, Zhaozhuo Xu, Shanshan Han, Han Jin, Alay Dilipbhai Shah, Dimitris Stripelis, Yuhang Yao, Salman Avestimehr, Tong Zhang, and Chaoyang He. Fox-1: Open small language model for cloud and edge, 2025. URL <https://arxiv.org/abs/2411.05281>.

Tosio Kato. *Perturbation Theory for Linear Operators*, volume 132 of *Grundlehren der mathematischen Wissenschaften*. Springer-Verlag, Berlin, Heidelberg, 2nd edition, 1980. ISBN 3-540-07558-5. URL <https://webhomes.maths.ed.ac.uk/~v1ranick/papers/kato1.pdf>.

Diederik P. Kingma and Jimmy Ba. Adam: A method for stochastic optimization, 2017. URL <https://arxiv.org/abs/1412.6980>.

Leo Kozachkov, Ksenia V. Kastanenka, and Dmitry Krotov. Building transformers from neurons and astrocytes. *Proceedings of the National Academy of Sciences*, 120(34):e2219150120, 2023. doi: 10.1073/pnas.2219150120. URL <https://www.pnas.org/doi/abs/10.1073/pnas.2219150120>.

Zorah Lähner and Michael Moeller. On the direct alignment of latent spaces. In *Proceedings of UniReps: the First Workshop on Unifying Representations in Neural Models*, pages 158–169. PMLR, 2024.

Brenden Lake and Marco Baroni. Generalization without systematicity: On the compositional skills of sequence-to-sequence recurrent networks. In *International conference on machine learning*, pages 2873–2882. PMLR, 2018.

Mario Lezcano-Casado and David Martínez-Rubio. Cheap orthogonal constraints in neural networks: A simple parametrization of the orthogonal and unitary group, 2019. URL <https://arxiv.org/abs/1901.08428>.

Qing Li, Yixin Zhu, Yitao Liang, Ying Nian Wu, Song-Chun Zhu, and Siyuan Huang. Neural-symbolic recursive machine for systematic generalization. *arXiv preprint arXiv:2210.01603*, 2022.

Mitch Marcus, Beatrice Santorini, and Mary Ann Marcinkiewicz. Building a large annotated corpus of english: The penn treebank. *Computational linguistics*, 19(2):313–330, 1993.

Kanti V Mardia, John T Kent, and Charles C Taylor. *Multivariate analysis*. John Wiley & Sons, 2024.

Saeed Masoudnia and Reza Ebrahimpour. Mixture of experts: a literature survey. *Artificial Intelligence Review*, 42:275–293, 2014.

Jeff Mitchell and Mirella Lapata. Vector-based models of semantic composition. In *proceedings of ACL-08: HLT*, pages 236–244, 2008.

Jonas Pfeiffer, Sebastian Ruder, Ivan Vulić, and Edoardo Maria Ponti. Modular deep learning. *arXiv preprint arXiv:2302.11529*, 2023.

Mert Pilanci. From complexity to clarity: Analytical expressions of deep neural network weights via clifford’s geometric algebra and convexity, 2024. URL <https://arxiv.org/abs/2309.16512>.

Ofir Press, Muru Zhang, Sewon Min, Ludwig Schmidt, Noah A. Smith, and Mike Lewis. Measuring and narrowing the compositionality gap in language models, 2023. URL <https://arxiv.org/abs/2210.03350>.

Qwen, :, An Yang, Baosong Yang, Beichen Zhang, Binyuan Hui, Bo Zheng, Bowen Yu, Chengyuan Li, Dayiheng Liu, Fei Huang, Haoran Wei, Huan Lin, Jian Yang, Jianhong Tu, Jianwei Zhang, Jianxin Yang, Jiaxi Yang, Jingren Zhou, Junyang Lin, Kai Dang, Keming Lu, Keqin Bao, Kexin Yang, Le Yu, Mei Li, Mingfeng Xue, Pei Zhang, Qin Zhu, Rui Men, Runji Lin, Tianhao Li, Tianyi Tang, Tingyu Xia, Xingzhang Ren, Xuancheng Ren, Yang Fan, Yang Su, Yichang Zhang, Yu Wan, Yuqiong Liu, Zeyu Cui, Zhenru Zhang, and Zihan Qiu. Qwen2.5 technical report, 2025. URL <https://arxiv.org/abs/2412.15115>.

Daking Rai, Yilun Zhou, Shi Feng, Abulhair Saparov, and Ziyu Yao. A practical review of mechanistic interpretability for transformer-based language models. *arXiv preprint arXiv:2407.02646*, 2024.

Carlos Riquelme, Joan Puigcerver, Basil Mustafa, Maxim Neumann, Rodolphe Jenatton, André Susano Pinto, Daniel Keysers, and Neil Houlsby. Scaling vision with sparse mixture of experts. *Advances in Neural Information Processing Systems*, 34:8583–8595, 2021.

Martin Roelfs and Steven De Keninck. Graded symmetry groups: Plane and simple, 2021. URL <https://arxiv.org/abs/2107.03771>.

David Ruhe, Johannes Brandstetter, and Patrick Forré. Clifford group equivariant neural networks, 2023a. URL <https://arxiv.org/abs/2305.11141>.

David Ruhe, Jayesh K. Gupta, Steven de Keninck, Max Welling, and Johannes Brandstetter. Geometric clifford algebra networks, 2023b. URL <https://arxiv.org/abs/2302.06594>.

Sara Sabour, Nicholas Frosst, and Geoffrey E Hinton. Dynamic routing between capsules, 2017. URL <https://arxiv.org/abs/1710.09829>.

Simon Schug, Seijin Kobayashi, Yassir Akram, Maciej Wołczyk, Alexandra Proca, Johannes von Oswald, Razvan Pascanu, João Sacramento, and Angelika Steger. Discovering modular solutions that generalize compositionally, 2024. URL <https://arxiv.org/abs/2312.15001>.

Vikas Sindhwani, Tara Sainath, and Sanjiv Kumar. Structured transforms for small-footprint deep learning. *Advances in Neural Information Processing Systems*, 28, 2015.

Lars St, Svante Wold, et al. Analysis of variance (anova). *Chemometrics and intelligent laboratory systems*, 6(4):259–272, 1989.

Kai Sheng Tai, Richard Socher, and Christopher D Manning. Improved semantic representations from tree-structured long short-term memory networks. *arXiv preprint arXiv:1503.00075*, 2015.

Hugo Touvron, Thibaut Lavril, Gautier Izacard, Xavier Martinet, Marie-Anne Lachaux, Timothée Lacroix, Baptiste Rozière, Naman Goyal, Eric Hambro, Faisal Azhar, Aurelien Rodriguez, Armand Joulin, Edouard Grave, and Guillaume Lample. Llama: Open and efficient foundation language models, 2023. URL <https://arxiv.org/abs/2302.13971>.

Yifei Wang, Sungyoon Kim, Paul Chu, Indu Subramaniam, and Mert Pilanci. Randomized geometric algebra methods for convex neural networks, 2024. URL <https://arxiv.org/abs/2406.02806>.

Gail Weiss, Yoav Goldberg, and Eran Yahav. Thinking like transformers, 2021. URL <https://arxiv.org/abs/2106.06981>.

James H. Wilkinson. *The Algebraic Eigenvalue Problem*. Oxford University Press, Oxford, 1965.  
URL <https://doi.org/10.1017/S0013091500012104>.

Chenxi Yang and Swarat Chaudhuri. Safe neurosymbolic learning with differentiable symbolic execution, 2022. URL <https://arxiv.org/abs/2203.07671>.

Felix Yu, Sanjiv Kumar, Yunchao Gong, and Shih-Fu Chang. Circulant binary embedding. In *International conference on machine learning*, pages 946–954. PMLR, 2014.

Rowan Zellers, Ari Holtzman, Yonatan Bisk, Ali Farhadi, and Yejin Choi. Hellaswag: Can a machine really finish your sentence?, 2019. URL <https://arxiv.org/abs/1905.07830>.

Zhanpeng Zeng, Michael Davies, Pranav Pulijala, Karthikeyan Sankaralingam, and Vikas Singh. Lookupffn: making transformers compute-lite for cpu inference. In *International Conference on Machine Learning*, pages 40707–40718. PMLR, 2023.

Xiangyu Zhang, Xinyu Zhou, Mengxiao Lin, and Jian Sun. Shufflenet: An extremely efficient convolutional neural network for mobile devices, 2017. URL <https://arxiv.org/abs/1707.01083>.

Yanli Zhou, Reuben Feinman, and Brenden M Lake. Compositional diversity in visual concept learning. *Cognition*, 244:105711, 2024.

Andy Zou, Long Phan, Sarah Chen, James Campbell, Phillip Guo, Richard Ren, Alexander Pan, Xuwang Yin, Mantas Mazeika, Ann-Kathrin Dombrowski, Shashwat Goel, Nathaniel Li, Michael J. Byun, Zifan Wang, Alex Mallen, Steven Basart, Sanmi Koyejo, Dawn Song, Matt Fredrikson, J. Zico Kolter, and Dan Hendrycks. Representation engineering: A top-down approach to ai transparency, 2025. URL <https://arxiv.org/abs/2310.01405>.

## Appendix

In the Appendix, we provide additional discussions, formal proofs, and further experimental details that support the main paper. Section A outlines the limitations of this work. Section B presents the proofs of the algorithms and theorems, along with general results for certain special cases. Section C describes the hyperparameters and training setups used in the experiments. Section D includes additional experimental results.

### A Limitations

While our results demonstrate feasibility, they remain theoretical at this stage—though our rotor layers achieve competitive performance when replacing attention layers, the benefits are primarily in a radical parameter count reduction rather than immediate compute speedup in practice. Realizing such gains will require dedicated systems-level optimizations beyond the scope of this work.

Our current implementation relies on dense matrix representations of rotors and does not yet exploit the inherent sparsity of the rotor decomposition. Leveraging this sparsity will require new backpropagation schemes and software libraries, particularly when training from scratch. We discuss the matrix representation and sparse structure of rotors in detail in Section B.

Overall, this work is intended to highlight the feasibility and promise of decomposing linear layers—key building blocks in modern large models—into smaller (potentially geometric) modules, such as bivectors and rotors, to facilitate more compact and interpretable architectures.

## B Proofs

### B.1 Correctness Proofs for Main Algorithms

We prove the correctness of Alg. 1 and 2 in the theorems below.

**Theorem 2.** *Given a bivector  $b \in \text{Cl}^2(n)$ , a random vector  $v \in \text{Cl}^1(n)$  that has a non-zero component in the direction of the dominant simple component, and a threshold  $\epsilon \in \mathbb{R}$ , Alg. 2 returns an approximate simple projection of  $b$  in a differentiable way.*

*Proof.* Let  $B \in \mathfrak{so}(n)$  be the skew-symmetric matrix corresponding to  $b$ . We begin by showing that  $b \lrcorner v = Bv$  for any vector  $v$ . Fix an orthonormal basis  $\{e_1, \dots, e_n\}$  of  $\mathbb{R}^n$  and let

$$b = \sum_{1 \leq i < j \leq n} b_{ij}(e_i \wedge e_j) \quad \text{and} \quad v = \sum_{k=1}^n v_k e_k,$$

noting that  $[B]_{ij} = b_{ij}$  for  $1 \leq i < j \leq n$  and  $[B]_{ij} = -b_{ji}$  for  $1 \leq j < i \leq n$ . It is easy to verify that  $(e_i \wedge e_j) \lrcorner v = v_j e_i - v_i e_j$ . By bilinearity of the right contraction, we have

$$\begin{aligned} b \lrcorner v &= \sum_{i < j} b_{ij}(v_j e_i - v_i e_j) \\ &= \sum_{i < j} b_{ij}(v_j e_i) - \sum_{i < j} b_{ij}(v_i e_j) \\ &= \sum_{i < j} b_{ij}(v_j e_i) - \sum_{j < i} b_{ji}(v_j e_i) \quad \text{swapping } i \text{ and } j \\ &= \sum_{i < j} [B]_{ij}(v_j e_i) + \sum_{j < i} [B]_{ij}(v_j e_i) \\ &= \sum_i \sum_j [B]_{ij} v_j e_i = \sum_i (Bv)_i e_i = Bv. \end{aligned}$$

It follows that

$$b \lrcorner (b \lrcorner v) = b \lrcorner Bv = B^2 v = -B^T B v.$$

Since  $B^2$  is symmetric, we may apply the power iteration method. Observe, by skew-symmetry, the non-zero eigenvalues of  $B$  come in conjugate pairs

$$\{\pm i\sigma_1, \pm i\sigma_2, \dots, \pm i\sigma_k\},$$

with  $\sigma_1 \geq \sigma_2 \geq \dots \geq \sigma_k$  and  $k \leq \lfloor n/2 \rfloor$ . An associated orthonormal set of complex eigenvectors can be written as  $\{u_j \pm iv_j\}_{j \leq k}$ . Since  $\sigma_1$ , the dominant eigenvalue for  $B^2$ , has multiplicity 2, the power method on  $B^2$  will not converge in a single direction. Instead, it will *oscillate* within the two-dimensional span of  $\{u_1, v_1\}$  Wilkinson [1965].

Let  $v$  be one of the singular vectors on which the algorithm terminates. Since singular vectors are unique up to rotation, WLOG we choose  $v$  to be the right singular vector. Then, the left singular vector  $u$  and singular value  $\sigma$  satisfy  $b \llcorner v = Bv = \sigma u$  by definition.

By the Eckart-Young-Mirsky theorem [Golub and Van Loan, 2013], the best rank-2 approximation to  $B$  is its projection onto its simple two-dimensional subspace spanned by top two singular directions:

$$\text{Proj}_{\text{simple}}(b) = \sigma_1 u_1 v_1^T + \sigma_2 u_2 v_2^T.$$

As the singular values come in pairs for  $B$ , this reduces to  $\sigma_1(u_1 v_1^T + u_2 v_2^T)$ . But for  $B$ , the two right singular vectors  $v_1, v_2$  and the two left singular vectors  $u_1, u_2$  lie in the same two-plane, coming from the dominant eigenvalue conjugate pair,  $\pm i\sigma_1$ . Thus, we can choose  $u_2 = v_1$  and  $v_2 = -u_1$  (or vice versa), which ensures  $u_1 \perp v_1$  and  $u_2 \perp v_2$ . It follows that

$$\text{Proj}_{\text{simple}}(b) = \sigma_1(u_1 v_1^T - v_1 u_1^T) = \sigma_1(u_1 \wedge v_1).$$

Since Alg 2 solves only approximately for  $\sigma(u \wedge v) \approx \sigma_1(u_1 \wedge v_1)$ , we have that

$$\text{Proj}_{\text{simple}}(b) \approx \sigma_1(u_1 \wedge v_1).$$

Note that since the right contraction implementation is differentiable, Alg 2 is differentiable.  $\square$

**Theorem 3.** *Given  $b \in \text{Cl}^2(n)$  and  $k - 1$  many vectors  $v \in \text{Cl}^1(n)$ , Alg. 1 returns the invariant decomposition in a differentiable way.*

*Proof.* The heavy lifting is done by Eelbode et al. [2024] in Lem. 2, which states that  $b$  can be written as the sum of at most  $k$  commuting, orthogonal, simple bivectors

$$b = \sum_{j=1}^k \mu_j \frac{v_{\mu_j^+} \wedge v_{\mu_j^-}}{v_{\mu_j^+} \cdot v_{\mu_j^-}}$$

where  $\{\pm\mu_1, \pm\mu_2, \dots, \pm\mu_k\}$  is the spectrum of  $b$  and  $v_{\mu_j^+}$  and  $v_{\mu_j^-}$  are partner eigenvectors.

To obtain the full decomposition, it suffices to iteratively extract each term. If we have a differentiable subroutine to find the first term, then we can subtract it from  $b$ , apply the same routine to the residual, and repeat. Thus, it suffices to prove that the first term in the sum is equal to the projection of  $b$  onto the simple bivectors.

From the proof of Alg. 2, we know that

$$\text{Proj}_{\text{simple}}(b) = \sigma(u \wedge v)$$

where  $\sigma$  is the largest singular value and  $u, v$  are the corresponding left and right singular vectors. We wish to show that

$$\sigma(u \wedge v) = \mu_1 \frac{v_{\mu_1^+} \wedge v_{\mu_1^-}}{v_{\mu_1^+} \cdot v_{\mu_1^-}}.$$

The partner eigenvectors take the form  $v_{\mu_1^+} = u + iv$  and  $v_{\mu_1^-} = u - iv$ , as cited in the proof of Alg. 2. Then, the numerator reduces to

$$\begin{aligned} v_{\mu_1^+} \wedge v_{\mu_1^-} &= (u + iv) \wedge (u - iv) \\ &= u \wedge u - iu \wedge v + iv \wedge u + v \wedge u \\ &= -iu \wedge v + iv \wedge u \\ &= -2iu \wedge v. \end{aligned}$$

as the wedge product is antisymmetric. The denominator reduces to

$$\begin{aligned} v_{\mu_1^+} \cdot v_{\mu_1^-} &= (u + iv) \cdot (u - iv) \\ &= u \cdot u - iu \cdot v + iv \cdot u + v \cdot v \\ &= u \cdot u + v \cdot v \\ &= 2 \end{aligned}$$

as singular vectors are orthonormal. Since  $\mu_1 = i\sigma$ , we have that

$$\mu_1 \frac{v_{\mu_1^+} \wedge v_{\mu_1^-}}{v_{\mu_1^+} \cdot v_{\mu_1^-}} = i\sigma \frac{-2iu \wedge v}{2} = \sigma(u \wedge v) = \text{Proj}_{\text{simple}}(b),$$

as desired. Subtraction is differentiable and as  $\text{Proj}_{\text{simple}}(b)$  can be found in a differentiable way, this algorithm is differentiable.  $\square$

## B.2 Parameter Count

We revisit the main theorem on the parameter count for rotor maps and provide a proof of the statement.

**Theorem 4** ( $\psi$  Parameter Count). *Let  $\psi : \mathbb{R}^{d_{in}} \rightarrow \mathbb{R}^{d_{out}}$  be a linear map composed of rotor modules  $\psi_{r_{ij}, s_{ij}}$  with  $i \in [c_1]$  and  $j \in [c_2]$ , each acting in  $\text{Cl}(n)$ . Let  $2^n \leq d \triangleq \min(d_{in}, d_{out})$ . Then, the total number of learnable parameters is upper bounded by*

$$2c_1c_2 \binom{n}{2} = \mathcal{O}(\log^2 d).$$

*Proof.* Each rotor is the exponential of a bivector. As general bivectors are a linear combination of basis bivectors, of which there are  $\binom{n}{2}$ , parametrizing a bivector takes  $\binom{n}{2}$  scalar parameters. Hence, a single rotor-sandwich map  $\psi_{r_{ij}, s_{ij}}$  is parametrized using  $2\binom{n}{2}$  scalar parameters. The result is then immediate, since there are  $c_1c_2$  such modules, corresponding to all input and output pairs.  $\square$

Tab. 6 summarizes the number of parameters required for each key, query, and value projection per attention layer using different replacement methods across all LLMs used in our experiments.

## B.3 Technical Analysis of Matrix Representation of Rotor Application

We implement the sandwich product in (2), along with other operations such as grade-restricted wedge and inner products, using the `torch_ga` Clifford algebra package for PyTorch, available at Alesiani [2023]. In our implementation of (2), the rotor action is represented by a matrix  $M$ . In this section, we describe the construction of  $M$  and introduce some of its key properties. These results highlight the special orthogonality and block structure of  $M$ . While the two-rotor map  $\psi_{r,s}(x)$  in (6) does not satisfy these properties exactly, it appears to share similar properties and structure; we do not discuss it here.

We compute the sandwich product using a change-of-basis matrix.

**Definition 2.** *Let  $r \in \text{Spin}(n)$ , and let  $\{e_J\}_{J \subseteq [n]}$  denote the canonical basis of  $\text{Cl}(n)$  (where  $J$  is an ordered multi-index). Define*

$$N_r = [\tau(\psi_r(e_J))]_{J \subseteq [n]},$$

where  $\psi_r(x) = rxr^\dagger$  and  $\tau$  is the canonical vector-space isomorphism  $\tau : \text{Cl}(n) \rightarrow \mathbb{R}^{2^n}$ . That is, each row of  $N_r$  is the coefficients of  $re_Jr^\dagger$  expressed in the basis. We refer to  $N_r$  as the change-of-basis matrix for  $r$ .

**Lemma 3.** *Let  $x \in \text{Cl}(n)$ ,  $r \in \text{Spin}(n)$ , and  $N_r$  be defined as in Def. 2. Then, the two mappings*

$$x \mapsto xN_r \quad \text{and} \quad x \mapsto rxr^\dagger$$

*are the same linear map up to isomorphism.*

*Proof.* Write  $x$  as

$$x = \sum_{J \subseteq [n]} x_J e_J,$$

where  $x_J$  is the real coefficient of the basis element  $e_J$ . Let  $\tau : \text{Cl}(n) \rightarrow \mathbb{R}^{2^n}$  be the canonical vector-space isomorphism that gives the row vector coordinates of the multivector,  $\phi_r(x) = rxr^\dagger$  for  $x \in \text{Cl}(n)$ , and  $\delta(y) = yN_r$  for  $y \in \mathbb{R}^{2^n}$ . To prove  $\phi$  and  $\delta$  are the same up to isomorphism, we must prove that  $\tau(\phi_r(x)) = \delta(\tau(x))$  for all  $x \in \text{Cl}(n)$ .

For each basis element  $e_J$ , the sandwich product gives some multivector  $\psi(e_J) = re_Jr^\dagger$ , which we express as

$$re_Jr^\dagger = \sum_{I \subseteq [n]} [N_r]_{J,I} e_I,$$

since  $(N_r)_{J,I}$  stores the coefficient of  $e_I$  in  $re_Jr^\dagger$  by definition. Then,

$$\begin{aligned} \tau(\phi_r(x)) &= \tau(rx r^\dagger) \\ &= \tau\left(r\left[\sum_{J \subseteq [n]} x_J e_J\right] r^\dagger\right) \\ &= \tau\left(\sum_{J \subseteq [n]} x_J r e_J r^\dagger\right) \\ &= \tau\left(\sum_{J \subseteq [n]} x_J \left[\sum_{I \subseteq [n]} [N_r]_{J,I} e_I\right]\right) \\ &= \tau\left(\sum_{I \subseteq [n]} \left[\sum_{J \subseteq [n]} x_J [N_r]_{J,I}\right] e_I\right) \\ &= \sum_{I \subseteq [n]} \left[\sum_{J \subseteq [n]} x_J [N_r]_{J,I}\right] \tau(e_I) \quad \text{by linearity} \\ &= \tau(x) N_r \\ &= \delta(\tau(x)) \end{aligned}$$

where the second to last step follows as the inner sum is the dot product of  $\tau(x)$  with the  $I$ th column of  $N_r$ .  $\square$

This allows us to compute the rotor sandwich product via matrix multiplication. However, this gives us very little insight into the structure of  $N_r$  itself. For one,  $N_r$  must respect the grade-preserving property of rotors, meaning it is a block diagonal matrix. The following alternative view provides more insight into its structure.

**A more revealing view of  $N_r$ .** Let  $b \in \text{Cl}^2(n)$  be the bivector associated with  $r \in \text{Spin}(n)$  by  $r = \exp(b)$ , and let  $B \in \mathfrak{so}(n)$  be the corresponding skew-symmetric matrix. Let  $R \triangleq \exp(2B) \in \text{SO}(n)$  via the matrix exponential map. For each grade  $0 \leq k \leq n$ , set

$$M_k \triangleq C_k(R) \in \mathbb{R}^{\binom{n}{k} \times \binom{n}{k}},$$

where  $C_k(R)$  is the  $k$ th compound matrix of  $R$ . Algebraically,  $C_k(R)$  is the  $k$ th exterior power of  $R$ , i.e., the unique linear map  $\bigwedge^k(R)$  such that

$$\bigwedge^k(R)(m_1 \wedge m_2 \wedge \cdots \wedge m_k) = Rm_1 \wedge Rm_2 \wedge \cdots \wedge Rm_k$$

for all  $m_i \in \mathbb{R}^n$  for  $i \in [k]$  [Conrad, n.d.].

**Definition 3.** Let  $M_k$  be the  $k$ th compound, or exterior power, of  $R$ . Stack the  $M_k$  on the diagonal to form

$$M \triangleq \text{diag}(M_0, M_1, \dots, M_n) \in \mathbb{R}^{2^n \times 2^n}.$$

We first show that  $N_r$  and  $M$  are in fact the same matrix.

**Theorem 5.** Let  $N_r$  and  $M$  be defined as in Def. 2 and 3. Then,  $M = N_r$ .

*Proof.* The rotor sandwich product is a grade-preserving automorphism, implying  $\psi_r(\text{Cl}^k(n)) = \text{Cl}^k(n)$ . Thus,  $N_r$  is block-diagonal, one block per grade. First, we show  $\psi_r(v) = Rv$  for a vector  $v$ , where  $R = \exp(2B)$ . Observe

$$rvr^\dagger = e^b v (e^b)^\dagger = e^b v e^{b^\dagger} = e^b v e^{-b},$$

where the second equality follows as reversion is an anti-automorphism and the third equality follows as  $b^\dagger = -b$ . Now, consider the adjoint operator in an associative algebra defined as  $\text{ad}_X(Y) \triangleq [X, Y] = XY - YX$ . The Hadamard lemma and Talyer expansion together imply

$$e^b v e^{-b} = \sum_{k \geq 0} \frac{1}{k!} (\text{ad}_b)^k(v) = \exp(\text{ad}_b)v.$$

We also note the following identity:

$$\text{ad}_b(v) = bv - vb = (b \cdot v + b \wedge v) - (v \cdot b + v \wedge b) = 2b \cdot v = 2Bv,$$

where  $B$  is the skew-symmetric matrix for  $b$ . Putting these together, it follows that  $\psi_r(v) \triangleq rvr^\dagger = \exp(2B)v = Rv$ . Now, consider any  $k$ -vector  $v = e_{i_1} \wedge \cdots \wedge e_{i_k}$ . We have

$$\begin{aligned} \psi_r(v) &= \psi(e_{i_1}) \wedge \cdots \wedge \psi(e_{i_k}) & \psi_r \text{ is a grade-preserving automorphism} \\ &= (Re_{i_1}) \wedge \cdots \wedge (Re_{i_k}) & \text{from above} \\ &= \bigwedge^k (R)(v). \end{aligned}$$

Since the mapping is unique, we are done.  $\square$

Note that this block-diagonal structure highlights the *grade-preserving behavior of rotors*. This motivates our design choice to allow grade-mixing in our gadget for more expressivity. In particular, we insert random permutations between rotor layers so that information can mix across different grade components of the input multivector. Now that we have an alternative characterization of the sandwich product, we analyze its structure and the space in which it lives. Below, we examine several structural properties of the matrix  $M$ .

**Property 1.** *The matrix  $M$  in Def. 3 is a block diagonal matrix with at most  $\binom{2n}{n}$  non-zero entries.*

*Proof.*  $M = N_r$  by Thm. 5 and so  $M$  is block diagonal. There are  $n + 1$  blocks, each of size  $\binom{n}{k} \times \binom{n}{k}$  for  $0 \leq k \leq n$ . Thus, the total number of non-zero entries is at most

$$\sum_{k=0}^n \binom{n}{k}^2 = \binom{2n}{n},$$

which is far less than the  $2^{2n}$  of a dense  $2^n \times 2^n$  matrix.  $\square$

**Property 2.** *For every grade  $0 \leq k \leq n$ , the block  $M_k = C_k(R)$  lies in  $\text{SO}(\binom{n}{k})$ . Consequently,  $M \in \text{SO}(2^n)$ .*

*Proof.* By assumption,  $B \in \mathfrak{so}(n)$ , and so  $\exp(2B) = R \in \text{SO}(n)$ . Taking the  $k$ th exterior power preserves orthogonality and a determinant of 1. For each  $k$ , the  $k$ th compound matrix  $M_k = C_k(R)$  is the matrix representation of the  $k$ th exterior power  $\bigwedge^k (R)$  with respect to the standard basis of  $k$ -vectors. Since  $R$  is orthogonal,  $\bigwedge^k (R)$  preserves the induced inner product on  $k$ -vectors, making  $M_k$  orthogonal. Moreover, since  $\det(R) = 1$ , we have  $\det(M_k) = \det(\bigwedge^k (R)) = (\det(R))^{\binom{k-1}{k-1}} = 1$ .

Therefore,  $M_k \in \text{SO}(\binom{n}{k})$  for all  $0 \leq k \leq n$ . To prove  $M \in \text{SO}(2^n)$ , we note that since  $M$  is block diagonal,  $M^T = \text{diag}(M_0^T, \dots, M_n^T)$  and so  $M^T M = I$  as the  $M_k$  are special orthogonal.  $\det(M) = 1$  as the determinant of block diagonal matrices is the product of the determinant of the blocks, meaning  $\det(M) = \prod_{k=0}^n \det(M_k) = \prod_{k=0}^n 1 = 1$ .  $\square$

Note that under this view, we obtain a map from  $\mathfrak{so}(n)$  to  $\mathrm{SO}(2^n)$  by first applying the surjective exponential map from  $\mathfrak{so}(n)$  to  $\mathrm{SO}(n)$ , and then lifting  $\mathrm{SO}(n)$  to  $\mathrm{SO}(2^n)$  via the exterior powers. This transformation enables an *exponential reduction in the number of parameters required to represent rotor layers*. We conclude by identifying the class of matrices which  $M$  belongs. The following is a simple but useful characterization. The group of invertible elements of  $\mathrm{Cl}(n)$  is

$$\mathrm{Cl}^\times(n) = \{a \in \mathrm{Cl}(n) \mid \exists a^{-1} \in \mathrm{Cl}(n) \text{ st. } aa^{-1} = a^{-1}a = 1\}.$$

Let

$$\phi : \mathrm{Cl}^\times(n) \rightarrow \mathrm{GL}(2^n, \mathbb{R})$$

be the mapping which assigns to each  $a \in \mathrm{Cl}^\times(n)$  its change-of-basis matrix  $N_a$ . Then for any  $N_r$  corresponding to  $r \in \mathrm{Spin}(n)$ ,

$$N_r \in \phi(\mathrm{Spin}(n)).$$

We now give a more refined version of Prop. 2.

**Property 3.** *Let  $\phi$  be defined as above. Then,*

$$\phi(\mathrm{Spin}(n)) = \mathrm{SO}(2^n) \cap \phi(\mathrm{Cl}^\times(n)).$$

*Proof.* The first direction,  $\phi(\mathrm{Spin}(n)) \subseteq \mathrm{SO}(2^n) \cap \phi(\mathrm{Cl}^\times(n))$ , is immediate. If  $r \in \mathrm{Spin}(n)$ , then by definition  $r$  is an invertible element in  $\mathrm{Cl}^+(n)$  which satisfies  $rr^\dagger = 1_s$  (where  $1_s$  denotes the scalar identity). Thus,  $\mathrm{Spin}(n) \subseteq \mathrm{Cl}^\times(n)$ , which implies  $\phi(\mathrm{Spin}(n)) \subseteq \phi(\mathrm{Cl}^\times(n))$ . Furthermore, Prop. 2 and Thm 5 state  $N_r \in \mathrm{SO}(2^n)$  for  $r \in \mathrm{Spin}(n)$ , which ensures  $\phi(\mathrm{Spin}(n)) \subseteq \mathrm{SO}(2^n)$ .

For the other direction  $\mathrm{SO}(2^n) \cap \phi(\mathrm{Cl}^\times(n)) \subseteq \phi(\mathrm{Spin}(n))$ , we start by taking an arbitrary element from the set on the LHS and show it must also be in the set on the RHS. Thus, we assume  $g \in \mathrm{Cl}^\times(n)$  (an invertible multivector) such that its corresponding matrix  $N_g = \phi(g)$  is in  $\mathrm{SO}(2^n)$ . We wish to show  $g \in \mathrm{Spin}(n)$ . To do this, it suffices to prove two conditions:  $gg^\dagger = 1_s$  (i.e.,  $g$  is unit-norm), and  $g \in \mathrm{Cl}^+(n)$  (i.e.,  $g$  is an even multivector).

The matrix  $N_g$  represents the linear transformation  $T_g(X) = gXg^\dagger$ . The condition  $N_g \in \mathrm{SO}(2^n)$  means that  $N_g$  is an orthogonal matrix with  $\det(N_g) = 1_s$ . We know that due to orthogonality,  $T_g$  preserves the canonical inner product on  $\mathrm{Cl}(n)$ . We define this inner product as  $\langle X, Y \rangle = \langle X^\dagger Y \rangle_0$ , where  $\langle \cdot \rangle_0$  denotes the scalar part of a multivector.

We will first show that  $g^\dagger g = 1_s$ . Since  $T_g$  is an orthogonal transformation w.r.t.  $\langle X, Y \rangle = \langle X^\dagger Y \rangle_0$ , it must satisfy  $T_g^* T_g = \mathrm{I}$ , where  $\mathrm{I}$  is the identity map and  $T_g^*$  is the adjoint of  $T_g$  w.r.t. the inner product. The adjoint  $T_g^*$  is given by  $T_g^*(Y) = g^\dagger Y g$ . This can be verified by checking the main property of an adjoint,  $\langle Y, T_g(X) \rangle = \langle T_g^*(Y), X \rangle$ :

$$\begin{aligned} \langle Y, T_g(X) \rangle &= \langle Y^\dagger (gXg^\dagger) \rangle_0 \\ &= \langle (g^\dagger Y^\dagger g) X \rangle_0 \quad (\text{cyclically permute multivectors inside} \\ &\quad \text{scalar part operation, } \langle MNP \rangle_0 = \langle PMN \rangle_0) \\ &= \langle (g^\dagger Y g)^\dagger X \rangle_0 \quad (\text{since } (ABC)^\dagger = C^\dagger B^\dagger A^\dagger \text{ and } (A^\dagger)^\dagger = A) \\ &= \langle T_g^*(Y), X \rangle. \end{aligned}$$

Now, applying the condition  $T_g^* T_g = \mathrm{I}$  means  $T_g^*(T_g(X)) = X$  for all  $X \in \mathrm{Cl}(n)$ . Substituting the explicit forms for  $T_g$  and  $T_g^*$ , we get

$$\begin{aligned} g^\dagger (gXg^\dagger) g &= X \\ (g^\dagger g) X (g^\dagger g) &= X. \end{aligned}$$

Let  $A = g^\dagger g$ . The equation becomes  $AXA = X$  for all  $X \in \mathrm{Cl}(n)$ . By the Wedderburn-Artin theorem Cohn [2003], the Clifford algebra  $\mathrm{Cl}(n, 0)$  is isomorphic to a matrix algebra (or a direct sum of two such algebras) over  $\mathbb{R}$ ,  $\mathbb{C}$ , or  $\mathbb{H}$ . In such matrix algebras (and hence in  $\mathrm{Cl}(n, 0)$  or its relevant simple components where  $A$  lives, noting  $A$  is even), if an element  $A$  satisfies  $AXA = X$  for all elements  $X$  of the algebra, then  $A$  must be a scalar multiple of the identity, specifically  $\pm 1_s$ . Therefore, we must have  $A = g^\dagger g = \pm 1_s$ .

Fix an orthonormal basis  $e_J$  (where  $J$  is an ordered multi-index). Note that  $e_J^\dagger e_J = 1_s$  for every  $e_J$ . Write  $g = \sum_J c_J e_J$  for scalar coefficients  $c_J \in \mathbb{R}$ . Then, the scalar part of  $g^\dagger g$  is  $\langle g^\dagger g \rangle_0 = \sum_J c_J^2$ .

Since  $g$  is invertible, we have  $g \neq 0$ , so at least one  $c_J \neq 0$ , making this sum strictly positive. Since  $g^\dagger g = \lambda \cdot 1_s$  (where  $\lambda = \pm 1_s$ ), its scalar part is  $\lambda$ . As this scalar part  $\langle g^\dagger g \rangle_0$  must be positive, we must conclude that  $\lambda = 1_s$ , so  $g^\dagger g = 1_s$ .

Next, we will show that  $gg^\dagger = 1_s$ . From the previous result,  $g^\dagger g = 1_s$ . This means  $g$  is invertible and its unique inverse is  $g^{-1} = g^\dagger$ . Then, we can write  $gg^\dagger = gg^{-1} = 1_s$ . This helps us establish the first condition required for  $g$  to be an element of  $\text{Spin}(n)$ .

Finally, we will need to show that  $g \in \text{Cl}^+(n)$  (i.e.,  $g$  is an even multivector). Since  $N_g \in \text{SO}(2^n)$ , we have  $\det(N_g) = 1_s$ . Since  $gg^\dagger = 1_s$ , it follows that  $g^\dagger = g^{-1}$ . The transformation can now be written as  $T_g(X) = gXg^{-1}$ , which is an inner automorphism of  $\text{Cl}(n)$  induced by  $g$ ; such transformations are algebra automorphisms, meaning that they preserve the algebraic product structure (i.e.,  $T_g(XY) = T_g(X)T_g(Y)$ ). The elements  $g$  that satisfy  $gg^\dagger = 1_s$  are known as versors. Versors who are products of an odd number of vectors (odd versors) are elements of  $\text{Pin}(n) \setminus \text{Spin}(n)$ , while those that are products of an even number of vectors (even versors) are elements of  $\text{Spin}(n)$ . Note that  $\text{Pin}(n)$  is the group of all such versors, and  $\text{Spin}(n) = \text{Pin}(n) \cap \text{Cl}^+(n)$ .

We know that if  $g$  were indeed an odd versor (an element of  $\text{Pin}(n) \setminus \text{Spin}(n)$ ), the induced inner automorphism  $X \mapsto gXg^{-1}$  when restricted to the vector subspace  $\text{Cl}^1(n)$  is an orthogonal transformation with determinant  $-1_s$  (as it includes a reflection, reversing orientation). It is a known result from the representation theory of Clifford algebras that the determinant of the full automorphism  $N_g : X \mapsto gXg^{-1}$  acting on the entire algebra  $\text{Cl}(n)$  corresponds to the parity of the versor  $g$ . Specifically,  $\det(N_g) = +1_s$  if  $g$  is an even versor (i.e.,  $g \in \text{Spin}(n)$ ), and  $\det(N_g) = -1_s$  if  $g$  is an odd versor (i.e.,  $g \in \text{Pin}(n) \setminus \text{Spin}(n)$ ). This directly links the parity of the versor  $g$  to the determinant of the full transformation matrix  $N_g$ . Since we know  $\det(N_g) = 1_s$ ,  $g$  must be an even versor, i.e.,  $g \in \text{Cl}^+(n)$ .

Since we have shown both  $gg^\dagger = 1_s$  and  $g \in \text{Cl}^+(n)$ , we must conclude that  $g \in \text{Spin}(n)$  by its definition. Thus,  $\text{SO}(2^n) \cap \phi(\text{Cl}^1(n)) \subseteq \phi(\text{Spin}(n))$ . □

Prop. 3 provides an alternative characterization of the group of matrices associated with rotor conjugation, i.e.,  $N_r$  lives in the intersection of the special orthogonal group and the subgroup of matrices defined by the group of units of  $\text{Cl}(n)$ .

## C Hyperparameters and Experiment Details

We detail the training configurations for all experiments involving Rotor, Low-Rank (LR), and Block-Hadamard (BH) projections used to approximate attention layers.

### C.1 Training Details

**Learning approximation layers in attention.** To approximate the linear projections in attention layers of an LLM, we train all replacement modules (Rotor, LR, or BH) by minimizing mean squared error (MSE) loss between the predicted and true projection outputs, based on latent representations extracted from LLMs.

Formally, let  $W \in \mathbb{R}^{d_{\text{out}} \times d_{\text{in}}}$  be the dense projection matrix (i.e., query, key, or value) we want to approximate within a transformer block. Given hidden input  $x \in \mathbb{R}^{d_{\text{in}}}$ , the projection computes  $y = Wx \in \mathbb{R}^{d_{\text{out}}}$ . To train an approximate layer, we collect a dataset  $\mathcal{D} = \{(x_i, y_i)\}_{i=1}^N$  by prompting the LLM with a set of prompts  $\{P_j\}_{j \leq n}$  (e.g., Arc Challenge) and extracting the relevant hidden states at the target layer. Since hidden states are available for each token position in a sequence for self-attention, we have  $N = nT$ , where  $T$  is the average prompt length. We then learn an approximate layer  $H_\theta$  (rotors, LR, or BH) by minimizing

$$\min_\theta \sum_{i=1}^N (H_\theta x_i - y_i)^2,$$

where  $\theta$  denotes the set of trainable parameters (e.g., bivector coefficients for rotors). Optimization is done via gradient descent using the Adam optimizer [Kingma and Ba, 2017].

We jointly replace the query, key, and value projections within an attention layer of a transformer block. In our experiments, we replace up to three such attention layers and evaluate the resulting

model on downstream tasks of perplexity and accuracy metrics across various prompt datasets. When replacing multiple attention layers—say, layers  $I < J < K$ —we train them sequentially in order: first  $I$ , then  $J$ , and finally  $K$ . For each layer, we first replace all earlier trained layers (e.g.,  $I$  before  $J$ ), and then extract the input-output data for training the new layer under this modified model. This is to ensure that each replacement layer is trained with respect to the distribution induced by preceding replacements. Also, whenever we replace layer  $L$ , we retrain the output linear projection  $\tilde{W}_o^L$  within the same attention block, using the same MSE and Adam optimizer for consistency.

| Model         | Key                     | Query                   | Value                   |
|---------------|-------------------------|-------------------------|-------------------------|
| LLaMA-3.2 1B  | $2048 \rightarrow 512$  | $2048 \rightarrow 2048$ | $2048 \rightarrow 512$  |
| LLaMA-3.2 3B  | $3072 \rightarrow 1024$ | $3072 \rightarrow 3072$ | $3072 \rightarrow 1024$ |
| Qwen-2.5 1.5B | $1536 \rightarrow 256$  | $1536 \rightarrow 1536$ | $1536 \rightarrow 256$  |
| Fox-1.0 1.6B  | $2048 \rightarrow 512$  | $2048 \rightarrow 2048$ | $2048 \rightarrow 512$  |

**Table 4:** Input/output hidden dimensions for key, query, and value projections in a single attention layer of different LLMs.

In Tab. 4, we summarize the input and output hidden dimension for different LLMs.

**Rotor networks.** We define the rotor-based transformation as:

$$\psi_{r,s}(x) \triangleq rxs^\dagger,$$

where  $r, s \in \text{Spin}(n)$ . Each rotor map is then composed as

$$\psi(x) \triangleq \sigma(\{\psi_{r_{ij}, s_{ij}}(x^{I_i}) \mid i \in [c_1], j \in [c_2]\}),$$

where  $\sigma$  is a pooling operator applied over the outputs of individual rotor transformation  $\psi_{r_{ij}, s_{ij}}$ . More details are given in Subsection 4.2. As discussed, each rotor is parameterized by a small number of bivector coefficients that encode geometric rotations, leading to significantly fewer learnable parameters compared to dense or baseline layers. A rotor layer is constructed by stacking multiple rotor maps in depth and arranging them in parallel across width. For example, with width 2 and depth 3, the layer contains 6 rotor maps, each parameterized independently. In our experiments, to reduce computational cost, we use at most width 2 and depth 3 for a rotor layer, which along with any up and down projection needed that is done by the generalized version in 4.2 sums up to roughly 1000 scalar parameters per projection (i.e., per Q/K/V) layer for LLaMA-3.2 1B, compared to 1-4M in original dense layers.

Each rotor map is followed by a sequence of fixed (i.e., parameter-free) permutations, normalizations, and a nonlinearity. Since rotor sandwich products are grade-preserving (see Section B), we apply fixed permutations to enable interaction across grades and increase expressivity. We found that normalization improves training stability.

Hyperparameters such as depth, width, learning rate, and weight decay are selected via grid search; the final values along with the values we explored are listed in Tab. 5. All Clifford algebraic operations, including exponentiation of simple bivectors and sandwich products, are implemented entirely in PyTorch using the `torch_ga` library Alesiani [2023], which supports differentiation. We modified several methods in this package to reduce memory usage. For example, the original package computes the geometric product using a very sparse three dimensional Cayley table of shape  $2^n \times 2^n \times 2^n$  [Hitzer, 2013]. However, since we only require the geometric product between a pure rotor and a multivector when computing the sandwich product, we discard all but  $1 + \binom{n}{2}$  parts of the third dimension, rather than keeping the full  $2^n$ .

**Low-rank approximations.** We use low-rank (LR) approximation as one of our baselines, following prior work such as Hu et al. [2021]. Given a dense matrix  $W \in \mathbb{R}^{d_{\text{out}} \times d_{\text{in}}}$ , we approximate it as the product of two lower-dimensional matrices:  $X \in \mathbb{R}^{d_{\text{out}} \times r}$  and  $Y \in \mathbb{R}^{r \times d_{\text{in}}}$ , such that

$$W \approx XY,$$

where  $r \ll d_{\text{in}}, d_{\text{out}}$ . This decomposition effectively constrains the rank of the approximation to at most  $r$ , capturing a low-rank subspace of the original operator. Low-rank approximations have been shown to be effective in downstream tasks, especially when applied as additive fine-tuning modules to frozen large pre-trained weights. They are also computationally efficient, requiring only  $\mathcal{O}(r(d_{\text{out}} + d_{\text{in}}))$  parameters and operations. In our experiments, we choose  $r = 1$  and  $r = 4$ , and LR1 requires roughly  $3 - 5 \times$  parameters than our rotor layers. Hyperparameters are listed in Tab. 5.

| Method              | Hyperparameter        | Values Explored          | Final Value |
|---------------------|-----------------------|--------------------------|-------------|
| Rotor               | Chunk Size            | 1024, 2048, 4096         | 2048        |
|                     | Depth                 | 1,2,3                    | 1 or 3      |
|                     | Width                 | 1,2,3                    | 1 or 2      |
|                     | Nonlinearity          | ReLU, PReLU, GELU        | PReLU       |
|                     | Normalization         | true, false              | true        |
|                     | Permutations          | true, false              | true        |
|                     | Learning rate         | 0.001, 0.005, 0.01, 0.05 | 0.05        |
|                     | $\ell^2$ weight decay | 0.001, 0.01, 0.1, 0      | 0           |
|                     | Batch size            | 16, 32, 64, 128, 256     | 64          |
| Low-Rank (LR)       | Cosine annealing      | true, false              | true        |
|                     | Learning rate         | 0.001, 0.005, 0.01, 0.05 | 0.01        |
|                     | $\ell^2$ weight decay | 0.001, 0.01, 0.1, 0      | 0           |
|                     | Batch size            | 16, 32, 64, 128, 256     | 256         |
| Block-Hadamard (BH) | Cosine annealing      | true, false              | true        |
|                     | Block number          | 64                       | 64          |
|                     | Learning rate         | 0.001, 0.005, 0.01, 0.05 | 0.01        |
|                     | $\ell^2$ weight decay | 0.001, 0.01, 0.1, 0      | 0           |
|                     | Batch size            | 16, 32, 64, 128, 256     | 256         |
| Cosine annealing    | Cosine annealing      | true, false              | true        |

**Table 5:** Hyperparameter settings used for each method.

**Block-Hadamard approximations.** We adopt the Block-Hadamard (BH) projection as another baseline. The idea is to alternate Hadamard transforms with learnable block-diagonal matrices, enabling a trade-off between expressivity and efficiency through the block size [Zeng et al., 2023]. Formally, it is defined as

$$W \approx \prod_{i=1}^m B_i H,$$

where each  $B_i$  is a learnable block-diagonal matrix with block size  $b$ , and  $H$  is a fixed Hadamard transform. This approximation requires only  $\mathcal{O}(b \cdot \max(d_{\text{in}}, d_{\text{out}}))$  parameters, and can be interpreted as analogous to grouped convolutions followed by channel shuffling [Zhang et al., 2017]. The parameter  $m$  controls the depth of the transformation. In our experiments, we use  $m = 1$  (i.e., BH1) to reduce parameter count as much as possible and match the scale of rotor-based models. Even with this minimal configuration, BH1 has 8-40 $\times$  more parameters than rotors in the case of LLaMA-3.2 1B. Specifically, we use the approximation  $W \approx BH$ , where  $B$  is a block-diagonal matrix composed of  $n$  rectangular blocks, each of height  $h = d_{\text{out}}/n$  and width  $w = d_{\text{in}}/n$  for the number  $n$  of blocks. Hyperparameters are listed in Tab. 5.

## C.2 Computational Resources for Experiments

The experiments for each LLaMa-3.2 1B and Qwen-2.5 1.5B each took around 1500 GPU hours, Fox-1.0 1.6B around 1000 GPU hours, and LLaMa-3.2 3B around 500 GPU hours for a total of around 4500 GPU hours. This was spread across 8 NVIDIA A100 PCIe GPUs with 40 GBs of HBM2 memory. Total time of execution was around 3 weeks of run-time across all 8 GPUs.

*A note on the execution time of the rotor gadget.* We have not optimized the current code for speed or memory. At inference time, rotor layers are implemented as dense matrix multiplications. Therefore, its runtime scales with the depth of the rotor layer used in the replacement. In our experiments, we used hyperparameters of at most depth 2 and width 3; with an optimized implementation, this will result in at most 2 $\times$  slowdown, since width is trivially parallelizable.

It is important to note that this corresponds to a direct implementation—we currently do not leverage the block sparsity structure described in Section B.3, as current software support is quite limited. Custom kernels have recently become available to *batch* matrix-matrix multiplication of different

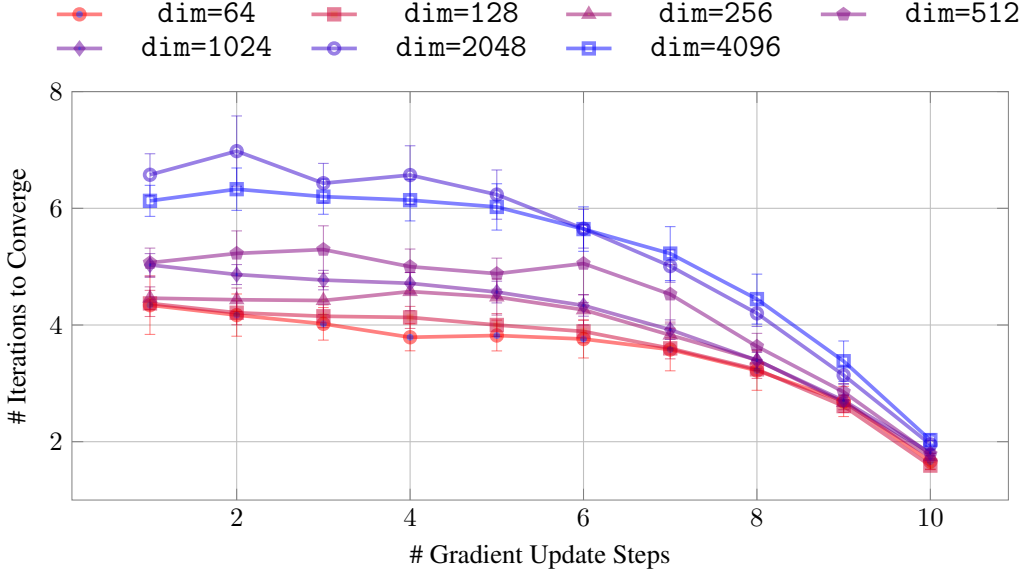


**Figure 6:** Number of iterations required by Alg 2 to converge within a tolerance of  $\epsilon = 10^{-3}$ , plotted against the number of gradient updates applied to the parameters of rotors (i.e., bivector coefficients). Results are averaged over 50 runs and simple bivectors in the invariant decomposition, with one standard deviation shown as error bars. The results demonstrate that warm-starting with previously learned singular vectors significantly accelerates convergence.

dimensions, such as those available in `cublasGemmGroupedBatchedEx`, but our setting requires vector-matrix multiplication. We found that this is slower than performing the dense implementation, though performance is expected to improve significantly once specialized vector-matrix versions become available. While custom kernels such as `cublasSgemmStridedBatched` support batching matrix-matrix multiplication of the *same* dimension, their adaptation to our rotors remains limited: even when applied to the parallel portions of our rotor gadget, they must operate sequentially on each block of the block sparse matrices. As a result, this gives a modest speedup, and there remains substantial room for further optimization.

## D Additional Experimental Results

In Fig. 6, we report the number of iterations required by Alg. 2 to converge within a tolerance of  $\epsilon = 10^{-3}$ , as a function of the number of gradient updates applied to the rotors (i.e., bivector coefficients). Synthetic data was generated with random input and having output come from the rotation corresponding to a random bivector. Each gradient update step is towards learning that random bivector with MSE loss. As expected, higher-dimensional projections require more iterations to converge. Notably, warm-starting from previously learned singular values significantly reduces the convergence speed across all dimensions, supporting our claim in Section 4.1.

In Tab. 7, 8, and 9, we provide additional experimental results on Qwen-2.5 1.5B, LLaMA-3.2 3B, and Fox-1-1.6B [Hu et al., 2025], where a single attention layer is replaced by our Rotor, LR1, LR4, or BH1 approximations. In Tab. 10, we provide averages for single and two-layer replacements for Fox-1-1.6B. The trends observed in the main paper persist: our rotor-based method consistently matches the baselines with significantly fewer parameters (see Tab. 6). These results further support our central claim: *linear layers can be synthesized from a small number of geometric primitives encoding rotations*.

| Model         | Method | Key          | Query        | Value        | Total        |
|---------------|--------|--------------|--------------|--------------|--------------|
| LLaMA-3.2 1B  | Dense  | 1,048,576    | 4,194,304    | 1,048,576    | 6,291,456    |
|               | LR1    | 2,560        | 4,096        | 2,560        | 9,216        |
|               | LR4    | 10,240       | 16,384       | 10,240       | 36,864       |
|               | BH1    | 8,192        | 32,768       | 8,192        | 49,152       |
|               | Rotor  | $\leq 1,080$ | $\leq 896$   | $\leq 1,080$ | $\leq 3,056$ |
| LLaMA-3.2 3B  | Dense  | 3,145,728    | 9,437,184    | 3,145,728    | 15,728,640   |
|               | LR1    | 4,098        | 6,148        | 4,098        | 14,344       |
|               | LR4    | 16,384       | 24,576       | 16,384       | 57,344       |
|               | BH1    | 32,768       | 98,304       | 32,768       | 163,840      |
|               | Rotor  | $\leq 1,080$ | $\leq 1,120$ | $\leq 1,080$ | $\leq 3,280$ |
| Qwen-2.5 1.5B | Dense  | 393,216      | 2,359,296    | 393,216      | 3,145,728    |
|               | LR1    | 1,792        | 3,072        | 1,792        | 6,656        |
|               | LR4    | 7,168        | 12,288       | 7,168        | 26,624       |
|               | BH1    | 4,096        | 24,576       | 4,096        | 32,768       |
|               | Rotor  | $\leq 904$   | $\leq 896$   | $\leq 904$   | $\leq 2,704$ |
| Fox-1.0 1.6B  | Dense  | 1,048,576    | 4,194,304    | 1,048,576    | 6,291,456    |
|               | LR1    | 2,560        | 4,096        | 2,560        | 9,216        |
|               | LR4    | 10,240       | 16,384       | 10,240       | 36,864       |
|               | BH1    | 8,192        | 32,768       | 8,192        | 49,152       |
|               | Rotor  | $\leq 1,080$ | $\leq 896$   | $\leq 1,080$ | $\leq 3,056$ |

**Table 6:** Number of parameters for key, query, and value projections in a single attention layer of each model, with the rightmost column showing their sum.

| Dataset           | Method | One layer replaced (Layer index) |       |       |       |       |       |       |       |       |       |       |       |       |       |
|-------------------|--------|----------------------------------|-------|-------|-------|-------|-------|-------|-------|-------|-------|-------|-------|-------|-------|
|                   |        | 1                                | 2     | 3     | 4     | 5     | 6     | 7     | 8     | 9     | 10    | 11    | 12    | 13    | 14    |
| Wikitext2 (↓)     | LR1    | 2.669                            | 2.330 | 2.351 | 2.354 | 2.332 | 2.316 | 2.350 | 2.340 | 2.326 | 2.315 | 2.381 | 2.311 | 2.514 | 2.306 |
|                   | LR4    | 2.635                            | 2.320 | 2.334 | 2.343 | 2.320 | 2.310 | 2.335 | 2.331 | 2.318 | 2.310 | 2.368 | 2.307 | 2.456 | 2.306 |
|                   | BH1    | 2.341                            | 2.316 | 2.329 | 2.323 | 2.323 | 2.308 | 2.338 | 2.321 | 2.314 | 2.307 | 2.354 | 2.308 | 2.417 | 2.307 |
|                   | Rotor  | 2.312                            | 2.299 | 2.305 | 2.312 | 2.308 | 2.298 | 2.301 | 2.315 | 2.303 | 2.300 | 2.321 | 2.304 | 2.320 | 2.301 |
| C4 (↓)            | LR1    | 3.129                            | 2.880 | 2.891 | 2.867 | 2.863 | 2.846 | 2.875 | 2.862 | 2.870 | 2.854 | 2.891 | 2.854 | 2.992 | 2.848 |
|                   | LR4    | 3.007                            | 2.880 | 2.890 | 2.869 | 2.862 | 2.846 | 2.873 | 2.862 | 2.867 | 2.854 | 2.888 | 2.853 | 2.939 | 2.848 |
|                   | BH1    | 2.943                            | 2.872 | 2.878 | 2.864 | 2.856 | 2.844 | 2.870 | 2.858 | 2.863 | 2.849 | 2.879 | 2.851 | 2.925 | 2.847 |
|                   | Rotor  | 2.892                            | 2.863 | 2.861 | 2.856 | 2.852 | 2.841 | 2.846 | 2.854 | 2.852 | 2.848 | 2.861 | 2.848 | 2.858 | 2.845 |
| PTB (↓)           | LR1    | 3.115                            | 3.034 | 3.063 | 3.073 | 3.011 | 3.023 | 3.081 | 3.031 | 3.033 | 3.023 | 3.102 | 3.019 | 3.173 | 3.018 |
|                   | LR4    | 3.110                            | 3.021 | 3.063 | 3.055 | 3.006 | 3.015 | 3.076 | 3.030 | 3.028 | 3.012 | 3.078 | 3.018 | 3.150 | 3.017 |
|                   | BH1    | 3.091                            | 3.007 | 3.046 | 3.044 | 3.004 | 3.007 | 3.076 | 3.020 | 3.022 | 3.007 | 3.064 | 3.015 | 3.101 | 3.012 |
|                   | Rotor  | 3.045                            | 2.998 | 3.018 | 3.025 | 3.001 | 2.998 | 3.014 | 3.015 | 3.008 | 3.003 | 3.028 | 3.012 | 3.034 | 3.009 |
| Arc Challenge (↑) | LR1    | 62.23                            | 63.95 | 59.23 | 47.21 | 60.52 | 66.52 | 52.36 | 58.37 | 57.51 | 50.21 | 40.34 | 58.80 | 22.32 | 57.51 |
|                   | LR4    | 59.66                            | 62.66 | 64.81 | 54.94 | 60.94 | 66.09 | 56.22 | 62.66 | 66.09 | 58.37 | 55.79 | 61.37 | 9.01  | 58.80 |
|                   | BH1    | 63.52                            | 64.38 | 58.80 | 60.04 | 62.23 | 63.09 | 62.66 | 63.52 | 65.24 | 60.94 | 58.88 | 59.66 | 53.22 | 50.21 |
|                   | Rotor  | 64.81                            | 67.38 | 65.61 | 62.23 | 62.66 | 64.38 | 61.80 | 63.95 | 65.24 | 66.09 | 62.23 | 64.81 | 60.09 | 56.22 |
| HellaSwag (↑)     | LR1    | 36.00                            | 47.00 | 45.00 | 46.67 | 50.00 | 51.00 | 50.33 | 44.00 | 17.33 | 36.00 | 46.00 | 52.67 | 31.33 | 20.00 |
|                   | LR4    | 38.00                            | 54.00 | 46.33 | 48.00 | 51.00 | 55.00 | 56.33 | 51.00 | 26.00 | 43.67 | 49.00 | 54.33 | 31.33 | 20.00 |
|                   | BH1    | 45.67                            | 48.00 | 46.00 | 48.33 | 48.67 | 50.67 | 51.67 | 52.33 | 38.33 | 44.67 | 48.00 | 51.33 | 24.33 | 32.67 |
|                   | Rotor  | 50.67                            | 53.00 | 53.67 | 52.33 | 52.00 | 55.33 | 57.00 | 54.67 | 48.67 | 55.33 | 51.00 | 57.00 | 51.33 | 32.00 |

| Dataset           | Method | One layer replaced (Layer index) |       |       |       |       |       |       |       |       |       |       |       |       |  |
|-------------------|--------|----------------------------------|-------|-------|-------|-------|-------|-------|-------|-------|-------|-------|-------|-------|--|
|                   |        | 15                               | 16    | 17    | 18    | 19    | 20    | 21    | 22    | 23    | 24    | 25    | 26    | 27    |  |
| Wikitext2 (↓)     | LR1    | 2.317                            | 2.304 | 2.314 | 2.317 | 2.323 | 2.316 | 2.331 | 2.316 | 2.309 | 2.301 | 2.409 | 2.300 | 2.316 |  |
|                   | LR4    | 2.317                            | 2.304 | 2.314 | 2.317 | 2.323 | 2.316 | 2.331 | 2.316 | 2.309 | 2.301 | 2.409 | 2.300 | 2.316 |  |
|                   | BH1    | 2.313                            | 2.301 | 2.314 | 2.316 | 2.320 | 2.311 | 2.311 | 2.315 | 2.309 | 2.300 | 2.398 | 2.297 | 2.309 |  |
|                   | Rotor  | 2.307                            | 2.299 | 2.302 | 2.309 | 2.308 | 2.307 | 2.306 | 2.311 | 2.304 | 2.296 | 2.358 | 2.295 | 2.308 |  |
| C4 (↓)            | LR1    | 2.866                            | 2.854 | 2.900 | 2.860 | 2.869 | 2.866 | 2.898 | 2.883 | 2.861 | 2.866 | 2.872 | 2.854 | 2.860 |  |
|                   | LR4    | 2.865                            | 2.851 | 2.899 | 2.859 | 2.868 | 2.866 | 2.889 | 2.866 | 2.856 | 2.851 | 2.858 | 2.853 | 2.858 |  |
|                   | BH1    | 2.862                            | 2.847 | 2.856 | 2.858 | 2.867 | 2.862 | 2.872 | 2.857 | 2.854 | 2.849 | 2.852 | 2.850 | 2.853 |  |
|                   | Rotor  | 2.855                            | 2.844 | 2.849 | 2.851 | 2.863 | 2.858 | 2.862 | 2.852 | 2.851 | 2.846 | 2.851 | 2.849 | 2.853 |  |
| PTB (↓)           | LR1    | 3.025                            | 3.003 | 3.020 | 3.021 | 3.036 | 3.019 | 3.086 | 3.010 | 3.014 | 3.012 | 3.019 | 3.061 | 3.098 |  |
|                   | LR4    | 3.024                            | 3.003 | 3.026 | 3.018 | 3.034 | 3.017 | 3.017 | 3.010 | 3.015 | 2.997 | 3.017 | 3.012 | 3.024 |  |
|                   | BH1    | 3.017                            | 3.000 | 3.008 | 3.014 | 3.029 | 3.012 | 3.010 | 3.009 | 3.011 | 2.995 | 3.015 | 3.005 | 3.016 |  |
|                   | Rotor  | 3.009                            | 2.998 | 3.003 | 3.006 | 3.019 | 3.008 | 3.008 | 3.001 | 3.007 | 2.993 | 3.012 | 3.001 | 3.011 |  |
| Arc Challenge (↑) | LR1    | 41.20                            | 65.24 | 27.90 | 65.24 | 68.24 | 16.31 | 47.64 | 67.38 | 66.95 | 65.67 | 65.24 | 66.09 | 66.52 |  |
|                   | LR4    | 31.76                            | 69.1  | 58.37 | 65.24 | 68.24 | 16.31 | 47.64 | 67.38 | 66.95 | 65.67 | 65.24 | 66.09 | 66.52 |  |
|                   | BH1    | 49.79                            | 68.67 | 48.50 | 62.23 | 62.24 | 42.49 | 48.93 | 65.24 | 67.81 | 64.39 | 65.31 | 65.79 | 65.24 |  |
|                   | Rotor  | 56.65                            | 70.82 | 61.37 | 60.09 | 69.53 | 51.07 | 47.21 | 67.81 | 66.52 | 66.09 | 65.67 | 66.09 | 65.24 |  |
| HellaSwag (↑)     | LR1    | 28.67                            | 49.67 | 32.67 | 45.67 | 51.00 | 5.67  | 36.33 | 52.67 | 57.33 | 53.33 | 53.67 | 53.67 | 54.67 |  |
|                   | LR4    | 28.67                            | 49.67 | 32.67 | 45.67 | 51.00 | 5.67  | 36.33 | 52.67 | 57.33 | 53.33 | 53.67 | 53.67 | 54.67 |  |
|                   | BH1    | 33.67                            | 56.67 | 45.67 | 45.67 | 53.33 | 22.67 | 37.67 | 53.67 | 53.67 | 47.67 | 52.33 | 56.00 | 51.67 |  |
|                   | Rotor  | 42.67                            | 55.00 | 49.33 | 51.33 | 52.67 | 18.67 | 35.00 | 51.00 | 56.67 | 54.00 | 54.33 | 54.00 | 56.67 |  |

**Table 7:** Performance on Log-PPL (↓) and accuracy (↑) when replacing **one attention layer** for layer indices 1–27 of Qwen-2.5 1.5B. Methods are Low Rank ( $r = 1$  and 4), BH1, and our Rotor. Original Log-PPL and Accuracy are: Wikitext2 2.287, C4 2.834, PTB 2.985, Arc Challenge 66.09, Hellaswag 55.00.

| Dataset       | Method | One layer replaced (Layer index) |       |       |       |       |       |       |       |       |       |       |       |       |       |
|---------------|--------|----------------------------------|-------|-------|-------|-------|-------|-------|-------|-------|-------|-------|-------|-------|-------|
|               |        | 1                                | 2     | 3     | 4     | 5     | 6     | 7     | 8     | 9     | 10    | 11    | 12    | 13    | 14    |
| Wikitext2 (↓) | LR1    | 3.867                            | 2.539 | 2.525 | 2.521 | 2.517 | 2.509 | 2.557 | 2.499 | 2.507 | 2.519 | 2.510 | 2.505 | 2.550 | 2.519 |
|               | LR4    | 3.389                            | 2.514 | 2.512 | 2.501 | 2.510 | 2.492 | 2.531 | 2.488 | 2.494 | 2.497 | 2.501 | 2.500 | 2.510 | 2.503 |
|               | BH1    | 2.552                            | 2.505 | 2.492 | 2.502 | 2.502 | 2.492 | 2.516 | 2.487 | 2.486 | 2.497 | 2.493 | 2.488 | 2.505 | 2.494 |
|               | Rotor  | 2.594                            | 2.520 | 2.497 | 2.499 | 2.517 | 2.498 | 2.521 | 2.488 | 2.492 | 2.511 | 2.499 | 2.492 | 2.506 | 2.510 |
| Wikitext2 (↓) | LR1    | 2.501                            | 2.487 | 2.481 | 2.473 | 2.487 | 2.484 | 2.477 | 2.479 | 2.487 | 2.489 | 2.490 | 2.479 | 2.519 |       |
|               | LR4    | 2.497                            | 2.485 | 2.477 | 2.471 | 2.480 | 2.479 | 2.471 | 2.467 | 2.480 | 2.474 | 2.471 | 2.471 | 2.503 |       |
|               | BH1    | 2.484                            | 2.479 | 2.476 | 2.471 | 2.472 | 2.475 | 2.466 | 2.469 | 2.477 | 2.476 | 2.475 | 2.469 | 2.482 |       |
|               | Rotor  | 2.488                            | 2.481 | 2.477 | 2.471 | 2.476 | 2.478 | 2.466 | 2.471 | 2.482 | 2.484 | 2.482 | 2.477 | 2.496 |       |

**Table 8:** Performance on Log-PPL (↓) and accuracy (↑) when replacing **one attention layer** for layer indices 1–27 of LLaMA-3.2 3B. Methods are Low Rank ( $r = 1$  and 4), BH1, and our Rotor. Original Log-PPL is 2.460.

| Dataset           | Method | One layer replaced (Layer index) |       |       |       |       |       |       |       |       |       |       |       |       |       |       |       |
|-------------------|--------|----------------------------------|-------|-------|-------|-------|-------|-------|-------|-------|-------|-------|-------|-------|-------|-------|-------|
|                   |        | 1                                | 2     | 3     | 4     | 5     | 6     | 7     | 8     | 9     | 10    | 11    | 12    | 13    | 14    | 15    | 16    |
| Wikitext2 (↓)     | LR1    | 2.645                            | 2.573 | 2.549 | 2.535 | 2.531 | 2.546 | 2.550 | 2.533 | 2.581 | 2.540 | 2.557 | 2.546 | 2.538 | 2.538 | 2.536 | 2.546 |
|                   | LR4    | 2.614                            | 2.568 | 2.538 | 2.535 | 2.530 | 2.544 | 2.545 | 2.531 | 2.570 | 2.538 | 2.552 | 2.535 | 2.538 | 2.538 | 2.536 | 2.534 |
|                   | BH1    | 2.633                            | 2.548 | 2.545 | 2.534 | 2.530 | 2.545 | 2.544 | 2.531 | 2.577 | 2.536 | 2.550 | 2.538 | 2.537 | 2.537 | 2.534 | 2.532 |
|                   | Rotor  | 2.544                            | 2.542 | 2.541 | 2.532 | 2.529 | 2.538 | 2.540 | 2.530 | 2.537 | 2.533 | 2.549 | 2.536 | 2.534 | 2.531 | 2.531 | 2.531 |
| C4 (↓)            | LR1    | 2.997                            | 2.915 | 2.879 | 2.877 | 2.877 | 2.891 | 2.884 | 2.878 | 2.889 | 2.886 | 2.876 | 2.884 | 2.874 | 2.881 | 2.878 | 2.875 |
|                   | LR4    | 2.960                            | 2.914 | 2.880 | 2.877 | 2.877 | 2.891 | 2.884 | 2.878 | 2.888 | 2.888 | 2.877 | 2.883 | 2.874 | 2.881 | 2.878 | 2.874 |
|                   | BH1    | 2.991                            | 2.901 | 2.875 | 2.878 | 2.876 | 2.891 | 2.881 | 2.878 | 2.889 | 2.879 | 2.874 | 2.876 | 2.872 | 2.879 | 2.877 | 2.872 |
|                   | Rotor  | 2.924                            | 2.901 | 2.875 | 2.876 | 2.876 | 2.890 | 2.881 | 2.878 | 2.882 | 2.878 | 2.873 | 2.876 | 2.872 | 2.878 | 2.876 | 2.871 |
| PTB (↓)           | LR1    | 3.359                            | 3.270 | 3.222 | 3.231 | 3.226 | 3.225 | 3.222 | 3.231 | 3.279 | 3.233 | 3.229 | 3.268 | 3.232 | 3.237 | 3.231 | 3.279 |
|                   | LR4    | 3.317                            | 3.259 | 3.215 | 3.231 | 3.225 | 3.260 | 3.224 | 3.230 | 3.276 | 3.232 | 3.229 | 3.235 | 3.230 | 3.242 | 3.229 | 3.226 |
|                   | BH1    | 3.318                            | 3.230 | 3.214 | 3.230 | 3.224 | 3.259 | 3.224 | 3.229 | 3.277 | 3.231 | 3.228 | 3.234 | 3.230 | 3.241 | 3.227 | 3.227 |
|                   | Rotor  | 3.283                            | 3.229 | 3.212 | 3.229 | 3.224 | 3.257 | 3.223 | 3.228 | 3.255 | 3.229 | 3.228 | 3.232 | 3.228 | 3.234 | 3.225 | 3.225 |
| Arc Challenge (↑) | LR1    | 31.76                            | 31.33 | 33.05 | 42.06 | 42.49 | 47.64 | 36.48 | 44.64 | 22.75 | 41.63 | 24.03 | 39.48 | 39.91 | 20.17 | 21.03 | 29.18 |
|                   | LR4    | 27.47                            | 26.61 | 27.90 | 36.91 | 39.06 | 48.50 | 36.05 | 41.20 | 15.45 | 35.19 | 18.88 | 31.33 | 42.06 | 16.74 | 21.03 | 23.61 |
|                   | BH1    | 34.33                            | 21.46 | 28.33 | 32.19 | 38.20 | 45.06 | 26.61 | 42.49 | 11.59 | 36.48 | 14.16 | 21.89 | 46.78 | 24.89 | 25.75 | 9.44  |
|                   | Rotor  | 27.04                            | 21.03 | 26.18 | 23.61 | 30.47 | 36.48 | 29.18 | 39.91 | 22.32 | 31.33 | 13.30 | 22.32 | 31.76 | 28.33 | 24.46 | 18.45 |
| HellaSwag (↑)     | LR1    | 31.33                            | 37.00 | 35.33 | 34.33 | 44.00 | 44.67 | 42.67 | 45.33 | 8.33  | 17.33 | 5.00  | 28.67 | 31.33 | 42.67 | 23.33 | 39.00 |
|                   | LR4    | 35.67                            | 36.67 | 25.00 | 33.00 | 42.67 | 43.33 | 43.00 | 44.67 | 6.33  | 19.00 | 4.33  | 26.67 | 31.33 | 41.33 | 18.67 | 39.33 |
|                   | BH1    | 40.00                            | 34.00 | 24.67 | 35.33 | 44.33 | 45.00 | 42.67 | 45.33 | 9.67  | 19.67 | 5.33  | 22.67 | 36.00 | 40.00 | 29.67 | 33.33 |
|                   | Rotor  | 40.00                            | 37.33 | 28.33 | 36.67 | 44.67 | 44.33 | 41.00 | 44.33 | 17.33 | 32.33 | 18.33 | 35.67 | 34.00 | 42.67 | 26.33 | 38.33 |
| Dataset           | Method | One layer replaced (Layer index) |       |       |       |       |       |       |       |       |       |       |       |       |       |       |       |
|                   |        | 17                               | 18    | 19    | 20    | 21    | 22    | 23    | 24    | 25    | 26    | 27    | 28    | 29    | 30    | 31    |       |
| Wikitext2 (↓)     | LR1    | 2.536                            | 2.530 | 2.564 | 2.553 | 2.534 | 2.544 | 2.546 | 2.523 | 2.537 | 2.522 | 2.535 | 2.617 | 2.540 | 2.544 | 2.571 |       |
|                   | LR4    | 2.534                            | 2.528 | 2.563 | 2.553 | 2.534 | 2.543 | 2.541 | 2.523 | 2.536 | 2.523 | 2.534 | 2.558 | 2.531 | 2.543 | 2.541 |       |
|                   | BH1    | 2.532                            | 2.528 | 2.558 | 2.550 | 2.530 | 2.538 | 2.537 | 2.521 | 2.530 | 2.521 | 2.532 | 2.556 | 2.529 | 2.539 | 2.532 |       |
|                   | Rotor  | 2.531                            | 2.527 | 2.531 | 2.548 | 2.529 | 2.538 | 2.534 | 2.521 | 2.529 | 2.521 | 2.531 | 2.553 | 2.528 | 2.537 | 2.531 |       |
| C4 (↓)            | LR1    | 2.879                            | 2.878 | 2.891 | 2.884 | 2.879 | 2.888 | 2.879 | 2.872 | 2.885 | 2.872 | 2.875 | 2.875 | 2.870 | 2.876 | 2.904 |       |
|                   | LR4    | 2.879                            | 2.877 | 2.891 | 2.884 | 2.880 | 2.889 | 2.879 | 2.872 | 2.884 | 2.872 | 2.874 | 2.875 | 2.870 | 2.875 | 2.890 |       |
|                   | BH1    | 2.878                            | 2.876 | 2.883 | 2.883 | 2.878 | 2.886 | 2.878 | 2.871 | 2.879 | 2.870 | 2.872 | 2.873 | 2.868 | 2.874 | 2.886 |       |
|                   | Rotor  | 2.877                            | 2.875 | 2.881 | 2.883 | 2.878 | 2.885 | 2.877 | 2.871 | 2.879 | 2.870 | 2.872 | 2.874 | 2.868 | 2.874 | 2.883 |       |
| PTB (↓)           | LR1    | 3.229                            | 3.233 | 3.253 | 3.246 | 3.220 | 3.237 | 3.227 | 3.218 | 3.248 | 3.221 | 3.219 | 3.249 | 3.220 | 3.242 | 3.264 |       |
|                   | LR4    | 3.224                            | 3.221 | 3.239 | 3.240 | 3.214 | 3.226 | 3.222 | 3.213 | 3.230 | 3.219 | 3.218 | 3.222 | 3.212 | 3.233 | 3.235 |       |
|                   | BH1    | 3.222                            | 3.222 | 3.238 | 3.239 | 3.214 | 3.226 | 3.222 | 3.210 | 3.230 | 3.217 | 3.217 | 3.222 | 3.212 | 3.221 | 3.226 |       |
|                   | Rotor  | 3.221                            | 3.220 | 3.232 | 3.238 | 3.213 | 3.225 | 3.220 | 3.210 | 3.228 | 3.216 | 3.217 | 3.220 | 3.211 | 3.220 | 3.223 |       |
| Arc Challenge (↑) | LR1    | 4.72                             | 6.87  | 39.91 | 44.21 | 18.45 | 33.91 | 34.33 | 21.46 | 7.30  | 27.47 | 18.88 | 29.18 | 47.64 | 10.30 | 7.73  |       |
|                   | LR4    | 6.87                             | 8.15  | 38.63 | 41.63 | 18.88 | 30.90 | 34.33 | 21.46 | 8.58  | 27.04 | 18.88 | 31.76 | 48.07 | 12.45 | 13.73 |       |
|                   | BH1    | 10.30                            | 5.58  | 35.62 | 42.49 | 20.17 | 30.04 | 32.19 | 24.03 | 9.87  | 25.32 | 19.31 | 25.32 | 46.78 | 18.88 | 24.46 |       |
|                   | Rotor  | 20.17                            | 18.88 | 25.32 | 33.91 | 21.03 | 30.04 | 26.61 | 24.46 | 11.59 | 26.18 | 21.46 | 24.89 | 45.49 | 19.74 | 24.46 |       |
| HellaSwag (↑)     | LR1    | 27.33                            | 26.33 | 42.33 | 47.33 | 41.33 | 37.00 | 37.67 | 32.00 | 23.67 | 40.00 | 34.67 | 46.67 | 47.33 | 28.67 | 12.00 |       |
|                   | LR4    | 25.00                            | 28.33 | 41.00 | 46.33 | 40.00 | 37.00 | 38.67 | 32.33 | 26.67 | 40.67 | 36.33 | 44.33 | 46.00 | 31.33 | 28.00 |       |
|                   | BH1    | 28.67                            | 27.67 | 42.33 | 47.67 | 44.00 | 40.67 | 38.33 | 34.67 | 27.33 | 39.67 | 36.67 | 42.33 | 47.00 | 32.33 | 36.67 |       |
|                   | Rotor  | 33.67                            | 34.00 | 33.00 | 34.67 | 37.67 | 41.00 | 38.33 | 34.33 | 29.67 | 39.67 | 33.67 | 40.67 | 46.33 | 31.67 | 38.67 |       |

**Table 9:** Performance on Log-PPL (↓) and accuracy (↑) when replacing **one attention layer** for layer indices 1–31 results of Fox-1.0 1.6B. Methods are Low Rank ( $r = 1$  and 4), BH1, and our Rotor. Original Log-PPL and Accuracy are: Wikitext2 2.517, C4 2.862, PTB 3.205, Arc Challenge 24.89, Hellaswag 38.33.

|              |               | Dataset  | Method   | Fox-1 1.6B |       |
|--------------|---------------|----------|----------|------------|-------|
|              |               |          |          | one        | two   |
| Log-PPL      | Wikitext2     | Original | Original | —          | 2.517 |
|              |               |          | LR1      | 2.550      | 2.589 |
|              |               |          | LR4      | 2.540      | 2.578 |
|              |               |          | BH1      | 2.538      | 2.573 |
|              | C4            | Rotor    | 2.534    | 2.576      |       |
|              |               |          | Original | —          | 2.862 |
|              |               |          | LR1      | 2.881      | 2.907 |
|              |               |          | LR4      | 2.880      | 2.901 |
| PTB          | BH1           | BH1      | 2.878    | 2.898      |       |
|              |               |          | Rotor    | 2.877      | 2.901 |
|              |               |          | Original | —          | 3.205 |
|              |               |          | LR1      | 3.238      | 3.299 |
|              | Rotor         | Rotor    | LR4      | 3.230      | 3.276 |
|              |               |          | BH1      | 3.228      | 3.275 |
|              |               |          | Rotor    | 3.226      | 3.259 |
|              |               |          | Original | —          | 24.89 |
| Accuracy (%) | Arc Challenge | Original | LR1      | 29.03      | 26.40 |
|              |               |          | LR4      | 27.40      | 27.12 |
|              |               |          | BH1      | 26.77      | 31.42 |
|              |               |          | Rotor    | 25.82      | 30.22 |
|              | HellaSwag     | Original | Original | —          | 38.33 |
|              |               |          | LR1      | 32.33      | 25.49 |
|              |               |          | LR4      | 32.41      | 24.40 |
|              |               |          | BH1      | 33.92      | 27.73 |
|              |               |          | Rotor    | 35.14      | 32.87 |

**Table 10:** Log PPL ( $\downarrow$ ) and accuracy ( $\uparrow$ ) using original, Low-Rank (1 or 4), BH1, and Rotor (ours) for 1–2 layer replacements on Fox-1 1.6B. One-layer results are averaged over all layers; two-layer results are averaged over five random selections. Red indicates best, blue second-best per setting.